POLITECNICO DI TORINO
Repository ISTITUZIONALE

Non-secular polariton leakage and dark-state protection in hybrid plasmonic cavities

Original
Non-secular polariton leakage and dark-state protection in hybrid plasmonic cavities / Vallone, M.. - In: NEW JOURNAL OF PHYSICS. - ISSN 1367-2630. - ELETTRONICO. - 28:9(2026). [10.1088/1367-2630/ae98a1]

Availability:
This version is available at: 11583/3015169 since: 2026-09-04T11:57:56Z

Publisher:
IOP

Published
DOI:10.1088/1367-2630/ae98a1

Terms of use:

This article is made available under terms and conditions as specified in the corresponding bibliographic description in the repository

Publisher copyright

(Article begins on next page)

28 October 2026

New Journal of Physics
The open access journal at the forefront of physics

Deutsche Physikalische Gesellschaft DPG
IOP Institute of Physics

Published in partnership with: Deutsche Physikalische Gesellschaft and the Institute of Physics

Check for updates

OPEN ACCESS

RECEIVED
30 January 2026

REVISED
23 April 2026

ACCEPTED FOR PUBLICATION
12 August 2026

PUBLISHED
4 September 2026

Original content from this work may be used under the terms of the Creative Commons Attribution 4.0 licence.

Any further distribution of this work must maintain attribution to the author(s) and the title of the work, journal citation and DOI.

PAPER

Non-secular polariton leakage and dark-state protection in hybrid plasmonic cavities

Marco Vallone*

Dipartimento di Elettronica e Telecomunicazioni, Politecnico di Torino, Corso Duca degli Abruzzi 24, 10129 Torino, Italy
* Author to whom any correspondence should be addressed.

E-mail: marco.vallone@polito.it

Keywords: plasmonics, open quantum systems, nonsecular quantum master equations

Abstract

A major issue in exploiting plasmonic cavities as key components in nanotechnology is the effect of radiative and absorption losses on their electrodynamic behavior. Treating them as open systems, we derive a time-local, completely positive master equation that retains non-secular interference between decay pathways and reduces to the standard secular description when the environment resolves polariton splitting. When it does not, the theory predicts order-one deviations from secular leakage dynamics, including bath-induced coherences and formation of a comparatively long-lived dark polaritonic component, and provides a simple design criterion based on the ratio of polariton splitting to reservoir linewidth. A time-resolved leakage measurement, such as transmission, reflectivity, or photoluminescence, can be used to observe these effects.

1. Introduction

Surface plasmons in resonant cavities enable deep-subwavelength field confinement and enhanced light–matter interaction by reducing the effective mode volume. By tailoring the cavity geometry and the optical response of metallic or highly doped semiconductor reflectors, the coupling strength can be tuned from the weak to the strong and ultrastrong regimes, with corresponding modifications of radiative damping and plasmonic lifetimes upon hybridization [1–8].

Periodic arrays of metallic nanoparticles or suitable metasurfaces can efficiently excite surface plasmon polaritons (SPPs) at a reflector–dielectric interface of resonant cavities, as shown in figure 1. In this work, we use the term *hybrid plasmonic cavity* in a specific and relatively narrow sense: a resonant structure in which an electromagnetic cavity (EC) mode hybridizes with an SPP mode supported by a metallic or heavily doped semiconductor interface, typically with the aid of a metasurface or nanoparticle array that enables efficient excitation of the SPP. The resulting EC–SPP hybridization produces upper (UP) and lower (LP) polaritons with Hopfield-like dispersion and eigenfrequencies $\omega_\pm$ [6, 9–11]. In this context, the SPP degree of freedom is not merely an auxiliary component, but the essential matterlike mode whose coupling to the cavity field gives rise to the observed splitting. This usage is narrower than some broader photonic–plasmonic uses of the same term in the literature, and we adopt it here to avoid ambiguity. Such hybrid modes have been demonstrated from the terahertz to the visible range [12–17], providing an experimentally accessible platform to study driven and dissipative polariton dynamics.

A unified quantum open-system description for hybrid plasmonic cavities was developed in [18] by combining a microscopic treatment of the dressed retarded photon propagator with a Gorini–Kossakowski–Sudarshan–Lindblad (GKSL) master equation [19–21] in the Markovian and secular (rotating-wave) limits. In that approach, the Dyson equation for the dressed propagator $D(\omega)$ in the random-phase approximation (RPA) yields a complex self-energy $\mathcal{S}(\omega) = \Sigma(\omega) - \mathrm{i}\Gamma(\omega)/2$ which, in the long-wavelength limit of the RPA, is proportional to the microscopic susceptibility $\chi(\omega)$ of the medium [1, 22]. The real part $\Sigma(\omega)$ renormalizes the hybrid eigenfrequencies (including the observed blueshift of the UP and LP resonances in the strong-coupling regime [6, 7, 17]), while the imaginary part sets absorption-induced linewidths $\Gamma(\omega)$ that enter the leakage terms; in the low-density and secular

© 2026 The Author(s). Published by IOP Publishing Ltd on behalf of the Institute of Physics and Deutsche Physikalische Gesellschaft

approximation this leads to linear rate equations for UP/LP populations and coherences with constant decay rates determined self-consistently from $\mathcal{S}(\omega)$.

More generally, non-secular dressed-state master equations, Bloch–Redfield (BR) approaches, and generalized Lindblad constructions for bosonic light–matter systems are well established in quantum optics and open-system theory [23–27]. Therefore, the present work should not be viewed as a new general formalism for open quantum systems, but rather as a system-specific specialization of those methods to an EC–SPP hybrid cavity, with an explicit microscopic connection between the dissipative kernel, the retarded photon propagator, and the Drude–Lorentz susceptibility of the medium. In this sense, our main aim is to identify the physically relevant secular-breakdown regime for this class of plasmonic cavities and to clarify its consequences in terms of leakage-induced bright and dark polaritonic channels.

Building on this broader literature, and in particular on the completely positive BR-to-GKSL construction of [26, 27], we describe the system dynamics using a time-local, completely positive, and trace-preserving quantum master equation (QME) that retains non-secular interference (cross-damping) between decay pathways. The secular approximation keeps only dissipative contributions that couple transition operators with the same Bohr frequency and neglects cross terms oscillating as $e^{\pm i(\omega_i-\omega_j)t}$, which average out when $|\omega_i-\omega_j|$ is large compared to the relevant dissipative rates and the inverse bath correlation time (i.e. the spectral width of the environment).

This distinction is especially important in hybrid plasmonic cavities because these systems are inherently lossy and often operate in regimes where the same material and geometric parameters that control strong EC–SPP hybridization also determine the reservoir linewidth. Consequently, the polariton splitting and the environmental spectral width may not be well separated. In this case, a secular treatment can miss interference between unresolved leakage pathways and thus misestimate both decay dynamics and coherence generation. This is not just a formal issue; it directly affects experimentally relevant tasks such as linewidth engineering, selective enhancement or suppression of radiative leakage, and the possible emergence of a comparatively long-lived dark polaritonic component.

Our formulation therefore extends beyond the standard secular GKSL description in a regime of direct practical interest, specifically when the upper–lower polariton separation $\Delta=\omega_+-\omega_-$ is not resolved on the bath linewidth scale γ_D. In this system-specific context, the added value lies not in the general construction itself, but in the explicit link between the microscopic EC–SPP model, the reservoir linewidth, and the resulting dissipative crossover. In this regime, cross-damping renders the Kossakowski matrix nearly rank one, so the dissipation eigenchannels become collective bright and dark linear combinations of the underlying UP and LP transitions. In the present linear bosonic setting, the significance of this dark combination is not tied to emitter nonlinearity, but to dissipation engineering: leakage is redistributed between bright and dark channels, radiative decay can be selectively suppressed, and a comparatively longer-lived polaritonic component can emerge. These effects can be accessed directly through linear optical observables such as time-resolved transmission, reflectivity, or photoluminescence.

Moreover, the dark combination can become quasi-protected, leading to significant quantitative deviations from secular leakage models. Related interference-protected dark polaritonic modes have been discussed in other bosonic settings [28, 29], while experimental evidence in a more directly polaritonic solid-state platform has been reported in [30].

It is important to emphasize that the regime of interest does not, in principle, require ultrastrong coupling. The relevant condition is instead the unresolved-transition regime, $\Delta \lesssim \gamma_D$, meaning that the UP–LP splitting is not resolved on the bath-correlation scale. This can occur either because the splitting is moderate or because the reservoir linewidth is broad, so the decisive parameter is the ratio Δ/γ_D rather than the absolute coupling strength alone. At the same time, realistic plasmonic and related cavity platforms can indeed exhibit very large light–matter splittings together with broad linewidths: for example, ambient-condition nanoparticle-plasmon/cavity-photon systems have reached the ultrastrong-coupling regime [6], while 'epsilon-near-zero' nanocavity plasmon–phonon platforms have reported modal splittings up to about 50% of the resonant frequency [7]. These examples motivate the present EC–SPP setting, even though the secular-breakdown criterion discussed here is not restricted to the ultrastrong-coupling regime.

From an experimental perspective, the predicted crossover can be observed in time-resolved transmission, reflectivity, or photoluminescence measurements by tuning the UP–LP frequency separation across the boundary between the resolved regime, $\Delta \gg \gamma_D$, and the unresolved regime, $\Delta \lesssim \gamma_D$. In practice, this tuning can be achieved by varying the cavity detuning, light–matter coupling strength, or metasurface geometry, while monitoring the redistribution of leakage between bright and dark polaritonic channels.

It is important to note that the present theory applies more broadly to resonant systems in which a photonic mode interacts with matter excitations. This setting includes, for example, exciton–polaritons

in semiconductor microcavities, intersubband polaritons in quantum wells, phonon–polaritons in polar dielectrics, two-level atoms interacting with an optical field, and plasmonic nanocavities as in the considered case [5–8, 17, 31, 32].

The paper is organized as follows. In section 2 we review the hybrid plasmonic cavity model and its EC–SPP Hopfield diagonalization, and we show how the Dyson equation yields complex polariton eigenfrequencies $\omega_\pm$ with shifts Σ and linewidths Γ set by the microscopic Drude–Lorentz susceptibility. In section 3 we formulate the driven–dissipative master equation in the polariton basis with a leakage dissipator constructed without the secular approximation and cast the dynamics in a vectorized Liouvillian form for numerical simulations. In section 4 we compare the resulting non-secular dynamics with its secular approximation and discuss how bright and dark polaritons reveal interference effects and bath-induced coherence. We also suggest useful design criteria and approximate, analytical expressions for steady-state populations in the two compared descriptions, discussing their domain of validity. Section 5 summarizes the results and outlines possible extensions. Throughout we set $\hbar = c = k_\mathrm{B} = 1$; in the numerical results we express times in ps and frequencies in ps^{-1}.

2. Hybrid plasmonic cavity and polaritonic modes

Among the possible resonant cavities to which the formalism can be applied, we focus here on a specific type of hybrid plasmonic cavity, schematically shown in figure 1. In this model, the resonant structure consists of an EC mode at frequency ω_c strongly coupled to a SPP mode at frequency ω_pl, supported at a metallic or heavily doped semiconductor reflector or interface. The SPP mode is thus the matterlike degree of freedom responsible for the UP–LP splitting, rather than a secondary plasmonic perturbation of an otherwise purely photonic cavity.

In the Power–Zienau–Woolley multipolar picture [33, 34], the Hamiltonian describing the cavity as an isolated system without losses is given by

$$\hat{H}_\mathrm{s} = \omega_\mathrm{c}\left(\hat{a}^\dagger\hat{a} + \tfrac{1}{2}\right) + \omega_\mathrm{pl}\left(\hat{b}^\dagger\hat{b} + \tfrac{1}{2}\right) - \frac{\mathrm{i}\xi\Omega_\mathrm{pl}}{2}\left(\hat{a} - \hat{a}^\dagger\right)\left(\hat{b} + \hat{b}^\dagger\right) + \frac{\xi^2\Omega_\mathrm{pl}^2}{2}\left(\hat{b} + \hat{b}^\dagger\right)^2, \tag{1}$$

where $\hat{a}$ and $\hat{b}$ are EC and SPP bosonic annihilation operators, respectively, Ω_pl is the bulk plasma frequency, and $0 \leqslant \xi \leqslant 1$ is a dimensionless coupling constant [10, 11, 33]. The quadratic term $(\hat{b} + \hat{b}^\dagger)^2$ is the multipolar analogue of the $\mathbf{A}^2$ term which arises from minimal coupling (where $\mathbf{A}$ is the electromagnetic vector potential) and is responsible for the experimentally observed blue shift of the polariton branches at strong coupling [5–8, 33].

Diagonalizing $\hat{H}_\mathrm{s}$ by a Hopfield–Bogoliubov transform [9, 10] yields bosonic polariton operators $\hat{B}_\pm$, which obey $[\hat{B}_k, \hat{B}_l^\dagger] = \delta_{kl}$, such that

$$\hat{H}_\mathrm{s} = \omega_+\hat{B}_+^\dagger\hat{B}_+ + \omega_-\hat{B}_-^\dagger\hat{B}_-, \tag{2}$$

where $\omega_\pm$ are the UP and LP eigenfrequencies [22]

$$\omega_\pm^2 = 0.5\left(\omega_\mathrm{c}^2 + \widetilde{\omega}_\mathrm{pl}^2\right) \pm 0.5\sqrt{\left(\omega_\mathrm{c}^2 - \widetilde{\omega}_\mathrm{pl}^2\right)^2 + 4\Omega_\mathrm{pl}^2\omega_\mathrm{c}^2}, \tag{3}$$

and $\widetilde{\omega}_\mathrm{pl} = \sqrt{\omega_\mathrm{pl}^2 + \Omega_\mathrm{pl}^2}$.

In our previous work [18] we showed that, at the resonant crossing $\omega_\mathrm{pl} = \omega_\mathrm{c}$, the effect of the electronic medium and material losses on the cavity photon field can be equivalently described by the retarded photon propagator $D(\omega)$, which satisfies a Dyson equation of the form $D^{-1}(\omega) = D_0^{-1}(\omega) - \mathcal{S}(\omega)$, where $D_0(\omega)$ is the free cavity photon propagator. This formalism leads to an expression for $\omega_\pm$ given by

$$\omega_\pm = \omega_\mathrm{c} \pm \zeta + \Sigma - \mathrm{i}\Gamma/2, \tag{4}$$

where 2ζ quantifies the mode frequency separation (the Rabi frequency), $\Sigma = \mathrm{Re}[\mathcal{S}]$ is the energy renormalization, and $\Gamma = -2\,\mathrm{Im}[\mathcal{S}]$ defines the linewidth and depends on the losses due to absorption in the cavity (and possibly on radiative losses). In the long-wavelength limit of the RPA, the self-energy $\mathcal{S}$ is proportional to the complex electric susceptibility χ of the medium,

$$\chi(\omega) = \frac{\Omega_\mathrm{pl}^2}{\omega_\mathrm{pl}^2 - \omega^2 - \mathrm{i}\gamma_\mathrm{D}\omega}, \tag{5}$$

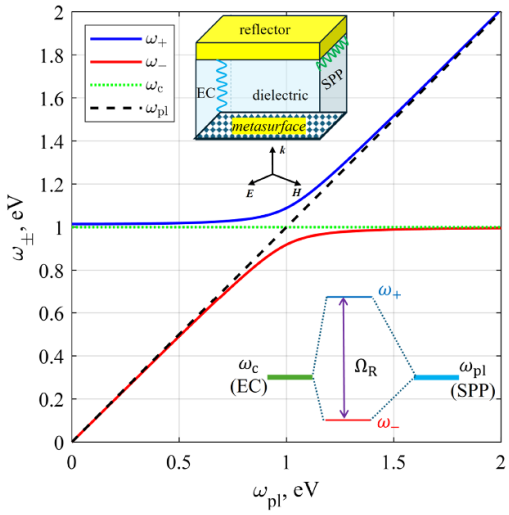

Figure 1. Schematic representation of EC–SPP hybridization and dispersion of eigenfrequencies $\omega_\pm$. The cavity is illuminated from below and supports an EC mode at ω_c. SPPs with frequency ω_{pl} are excited by a metasurface (e.g. a periodic lattice of nanoparticles) on the illuminated face of the cavity and propagate along the dielectric/reflector interface, which is assumed to be a medium-low loss material. The dispersion $\omega_\pm$ is calculated as in [22] for $\omega_c = 1$ eV, plasma frequency $\Omega_{pl} \approx 8.5$ eV, dimensionless EC–SPP coupling constant $\xi = 0.02$, and zero losses. Here and throughout, *hybrid plasmonic cavity* refers specifically to this EC-SPP hybridization setting.

where the rate γ_D accounts for SPP absorption in the medium [1, 2, 22]. Except for ω_c, all quantities in equation (4) depend explicitly on the losses, and their functional forms are briefly recalled in appendix A.

3. Driven–dissipative dynamics

The hybrid cavity can be conveniently described as a bosonic two-mode system, where the Fock states $|n_+, n_-\rangle$, with $n_\pm = 0, 1, 2, \ldots$, form an orthonormal basis for the Hilbert space of the isolated system (the vacuum corresponds to $n_+ = n_- = 0$). These states are generated from the vacuum by the upper (UP, +) and lower (LP, −) polariton creation operators $\hat{B}^\dagger_\pm$, and the corresponding number operators are $\hat{N}_\pm = \hat{B}^\dagger_\pm \hat{B}_\pm$. The Hamiltonian $\hat{H}_s$ of the isolated system, equation (2), is diagonal in this basis, with eigenvalues $E_{\mathbf{n}} \equiv E_{n_+,n_-} = n_+\omega_+ + n_-\omega_-$.

To investigate the cavity dynamics, we consider a time-dependent Hamiltonian of the form

$$\hat{H}(t) = \hat{H}_s + \hat{H}_{\text{drive}}(t), \tag{6}$$

where $\hat{H}_{\text{drive}}(t)$ accounts for external coherent drives. We model two types of coherent excitation: a cavity-like drive at frequency ω_c that populates the polariton modes, and a Raman-like drive with frequency ω_{ext} close to the UP–LP separation Δ, which coherently couples the two branches. They can be written in the Schrödinger picture as

$$\hat{H}_{\text{drive}}(t) = \sum_{k=\pm} \left[f_k \, e^{-i\omega_c t} \hat{B}^\dagger_k + f^*_k \, e^{i\omega_c t} \hat{B}_k \right] + \mathcal{R}_{\text{UP–LP}} \cos(\omega_{\text{ext}} t) \left(\hat{B}^\dagger_+ \hat{B}_- + \hat{B}^\dagger_- \hat{B}_+ \right), \tag{7}$$

where $f_\pm$ are complex drive amplitudes determined by the overlap between the cavity field and the polariton modes, and $\mathcal{R}_{\text{UP–LP}}$ controls the strength of the Raman-like interbranch coupling. Both drives can be switched on and off according to the designed simulation procedure. We also define the detuning $\delta = \Delta - \omega_{\text{ext}}$, although we usually focus on the resonant case $\delta = 0$ when discussing dark and bright modes in section 4.

We derive the dissipative generator for the undriven Hamiltonian $\hat{H}_s$ and include the external drive $\hat{H}_{\text{drive}}(t)$ *a posteriori* in the QME. The resulting evolution is written in the laboratory frame, and the interaction picture with respect to $\hat{H}_s$ is used only in the intermediate steps of the Born–Markov construction. This choice ensures that the leakage rates depend only on the Bohr spectrum of $\hat{H}_s$ and the bath spectral density. It is important to emphasize that the perturbative approximation underlying the Born–Markov construction concerns the coupling between the EC–SPP system and the bath, not the

coherent laser excitation itself. The latter is incorporated directly into the system Hamiltonian $\hat{H}_{\text{drive}}(t)$. Accordingly, when we later refer to a strong-driving regime, we mean a regime of larger coherent amplitudes within this effective Hamiltonian description, which can more substantially populate higher-excitation sectors, rather than a breakdown of the perturbative treatment of dissipation.

To account for dissipation, we consider four physical mechanisms: (i) leakage (radiative and/or absorptive) of the polariton modes, (ii) incoherent scattering from the upper to the lower polariton (UP→LP), (iii) incoherent scattering from the lower to the upper polariton (LP→UP), and (iv) pure dephasing of each polariton branch.

3.1. Leakage: mode absorption and radiative losses

The undriven Hamiltonian for the open system is written as $\hat{H}_{\text{s}} + \hat{H}_{\text{env}} + \hat{H}_{\text{int}}$, where $\hat{H}_{\text{env}}$ is the environment (or bath) Hamiltonian and $\hat{H}_{\text{int}}$ describes the system-bath interactions. We assume that the dominant leakage mechanism for both polariton branches is the interaction with a common electromagnetic reservoir, such as radiative leakage through the cavity boundaries or absorption in the reflector layer, therefore $\hat{H}_{\text{int}}$ can be written as

$$\hat{H}_{\text{int}} = \hat{X} \otimes \hat{\mathcal{B}}, \qquad \hat{X} = \hat{B}_+ + \hat{B}_- + \hat{B}_+^\dagger + \hat{B}_-^\dagger, \tag{8}$$

where $\hat{\mathcal{B}}$ is a bath operator that annihilates collective excitations in the electronic medium and in the external radiation continuum.

Following the standard BR formalism [21, 26, 35, 36], we expand $\hat{X}$ in terms of eigenoperators of $\hat{H}_{\text{s}}$,

$$\hat{X} = \sum_j A_j \hat{\sigma}_j + A_j^* \hat{\sigma}_j^\dagger, \qquad \hat{\sigma}_j = |n_j\rangle \langle m_j|, \tag{9}$$

where $|n_j\rangle$ and $|m_j\rangle$ are eigenstates of $\hat{H}_{\text{s}}$, and each $\hat{\sigma}_j$ is associated with a well-defined Bohr frequency $\omega_j = E_{m_j} - E_{n_j}$. Assuming the Fock states include no more than $N_{\max}$ excitations, they span a truncated Hilbert space $\mathcal{H}$ of dimension $d = (N_{\max} + 1)^2$, and the relevant transitions connect the vacuum to single-polariton states or, in higher sectors, differ by one excitation in either branch.

The bath is characterized by the correlation function $C(t) = \langle \hat{\mathcal{B}}(t)\hat{\mathcal{B}}(0)\rangle$ and by a rate-valued spectral density $J(\omega)$, related by the fluctuation–dissipation theorem to the dissipative part of the susceptibility [37–39]. Following [26], we model $J(\omega)$ as a Lorentzian centered at the SPP resonance ω_{pl} with full width at half maximum (FWHM) γ_{D},

$$J(\omega) = \Gamma_{\text{pl}} \frac{(\gamma_{\text{D}}/2)^2}{(\omega - \omega_{\text{pl}})^2 + (\gamma_{\text{D}}/2)^2}, \tag{10}$$

where $\Gamma_{\text{pl}} \equiv J(\omega_{\text{pl}})$ sets the peak leakage scale. The width γ_{D} controls the bath correlation time (and hence the suppression of cross-damping terms), while Γ_{pl} fixes the overall magnitude of the secular decay rates $\Gamma_\pm \equiv J(\omega_\pm)$; in this effective description they are independent parameters. On exact resonance, $\omega_{\text{pl}} = \omega_{\text{c}}$ and $\omega_\pm = \omega_{\text{pl}} \pm \Delta/2$, so the Lorentzian symmetry implies

$$\Gamma_\pm \equiv \Gamma = \Gamma_{\text{pl}} / \left[1 + (\Delta/\gamma_{\text{D}})^2\right]. \tag{11}$$

In the numerical simulations below, we set $\Gamma_{\text{pl}} = 2\gamma_{\text{D}}$ to fix the overall leakage timescale; this choice rescales absolute decay rates without reducing the generality.

Within the Born–Markov approximation, the BR master equation for the reduced density operator $\hat{\rho}(t)$ takes the form

$$\frac{\mathrm{d}\hat{\rho}}{\mathrm{d}t} = -\mathrm{i}\left[\hat{H}_{\text{s}}, \hat{\rho}\right] + \mathcal{K}_{\text{BR}}\hat{\rho}, \tag{12}$$

where the dissipative kernel $\mathcal{K}_{\text{BR}}$ can be expressed in the basis of transition operators $\{\hat{\sigma}_j\}$ as [21, 26]

$$\begin{aligned}\mathcal{K}_{\text{BR}}\hat{\rho} = \sum_{i,j} \Big\{ &-\mathrm{i}\left[\Lambda_{ij}(\omega_j)\,\hat{\sigma}_i^\dagger \hat{\sigma}_j \hat{\rho} - \hat{\rho}\,\Lambda_{ij}(\omega_i)\,\hat{\sigma}_i^\dagger \hat{\sigma}_j\right] + \mathrm{i}\left[\Lambda_{ij}(\omega_j) - \Lambda_{ij}(\omega_i)\right]\hat{\sigma}_j \hat{\rho} \hat{\sigma}_i^\dagger \\ &- \tfrac{1}{2}\left[W_{ij}(\omega_j)\,\hat{\sigma}_i^\dagger \hat{\sigma}_j \hat{\rho} + \hat{\rho}\,W_{ij}(\omega_i)\,\hat{\sigma}_i^\dagger \hat{\sigma}_j\right] + \tfrac{1}{2}\left[W_{ij}(\omega_j) + W_{ij}(\omega_i)\right]\hat{\sigma}_j \hat{\rho} \hat{\sigma}_i^\dagger \Big\}.\end{aligned} \tag{13}$$

Here, $W_{ij}(\omega)$ and $\Lambda_{ij}(\omega)$ are the decay and Lamb-shift matrices, respectively, given by $W_{ij}(\omega) = A_i^* A_j \gamma(\omega)$ and $\Lambda_{ij}(\omega) = A_i^* A_j \lambda(\omega)$, where the scalar functions $\gamma(\omega)$ and $\lambda(\omega)$ are determined by $J(\omega)$ as described in [21],

$$\gamma(\omega) = 2\pi\,\theta(\omega)\,J(\omega), \tag{14}$$

$$\lambda(\omega) = \mathcal{P}\int_0^\infty \mathrm{d}\omega' J(\omega')\left(\frac{1}{\omega-\omega'} + \frac{1}{\omega+\omega'}\right) \tag{15}$$

in the zero-temperature limit, where $\theta(\omega)$ is the Heaviside step function. This is a valid assumption, since the bath is approximately in the vacuum state or in a thermal state such that $k_\mathrm{B}T \ll \min_i(\omega_i)$, as commonly assumed in quantum optics [40]. For consistency, the numerical examples discussed below are also presented in the same zero-temperature limit for the leakage bath. It should also be noted, for clarity, that the bath operator $\hat{\mathcal{B}}$ appears only through the scalar functions $\gamma(\omega)$ and $\lambda(\omega)$ once the bath degrees of freedom have been traced out [41].

The key point of this approach is that both $W_{ij}(\omega)$ and $\Lambda_{ij}(\omega)$ inherit the full frequency dependence of $J(\omega)$, and therefore depend explicitly on the UP and LP frequencies $\omega_\pm$ and their separation Δ, describing the dynamics without invoking the secular approximation and including all possible couplings between populations and coherences.

However, the generator $-\mathrm{i}\left[\hat{H}_\mathrm{s},\cdot\right] + \mathcal{K}_\mathrm{BR}$ is not in Lindblad form and does not guarantee complete positivity of $\hat{\rho}(t)$. To obtain a Lindblad-like, completely positive master equation that preserves the non-secular physics captured by the BR equation, we follow the prescription proposed in [26], symmetrizing the frequency-dependent coefficients using an arithmetic mean for the Lamb-shift terms and a geometric mean for the dissipative terms:

$$\widetilde{\Lambda}_{ij} = \frac{\Lambda_{ij}(\omega_i) + \Lambda_{ij}(\omega_j)}{2}, \tag{16a}$$

$$\widetilde{W}_{ij} = \sqrt{W_{ij}(\omega_i)\,W_{ij}(\omega_j)} = \sqrt{J(\omega_i)J(\omega_j)}. \tag{16b}$$

Hereafter we absorb all frequency-independent prefactors (including the relevant system matrix elements) into the effective rate function $J(\omega)$, so that $W_{ii}(\omega_i) \equiv J(\omega_i)$ and the geometric-mean prescription can be written as in equation (16*b*).

The first choice ensures that the energy correction can be reorganized into a commutator with a Hermitian Lamb-shift Hamiltonian, while the second preserves the frequency dependence of the decay rates and strongly suppresses off-diagonal couplings when the corresponding Bohr frequencies are far apart compared to the bath linewidth.

Using the replacements equation (16) in equation (13), the QME can be written as

$$\frac{\mathrm{d}\hat{\rho}}{\mathrm{d}t} = -\mathrm{i}\left[\hat{H}_\mathrm{s} + \hat{H}_\mathrm{LS}, \hat{\rho}\right] + \mathcal{L}_{a\Lambda\text{–}gW}\hat{\rho}, \tag{17}$$

with the Lamb-shift Hamiltonian

$$\hat{H}_\mathrm{LS} = \sum_{i,j} \widetilde{\Lambda}_{ij}\,\hat{\sigma}_i^\dagger \hat{\sigma}_j \tag{18}$$

and the dissipator

$$\mathcal{L}_{a\Lambda\text{–}gW}\hat{\rho} = \sum_{i,j} \widetilde{W}_{ij}\left(\hat{\sigma}_j\hat{\rho}\hat{\sigma}_i^\dagger - \tfrac{1}{2}\left\{\hat{\sigma}_i^\dagger\hat{\sigma}_j, \hat{\rho}\right\}\right). \tag{19}$$

Equations (17)–(19) are in GKSL form provided that the dissipative kernel $\widetilde{W}_{ij}$ is positive semidefinite. Since the BR construction may produce a Hermitian Kossakowski matrix $\widetilde{W}$ with small negative eigenvalues, we diagonalize $\widetilde{W} = UDU^\dagger$, with U unitary and $D = \mathrm{diag}(d_1,\ldots,d_M)$ real, and enforce complete positivity by projecting onto the positive part: $d_\mu^{(+)} = \max(d_\mu, 0)$ and $\widetilde{W}_+ = UD^{(+)}U^\dagger$, where $D^{(+)} = \mathrm{diag}(d_1^{(+)},\ldots,d_M^{(+)})$. In the truncated polariton space used in section 4, the relevant leakage kernel reduces to a 2×2 matrix, whose eigenvalues (rates) and eigenvectors (jump operators) are given explicitly in that section (and in appendix B).

Introducing the jump operators $\hat{Q}_\mu = \sum_j U_{j\mu}\hat{\sigma}_j$, the master equation becomes

$$\frac{\mathrm{d}\hat{\rho}}{\mathrm{d}t} = -\mathrm{i}\left[\hat{H}_\mathrm{s} + \hat{H}_\mathrm{LS}, \hat{\rho}\right] + \mathcal{L}_\mathrm{leak}\,\hat{\rho} \tag{20a}$$

$$\mathcal{L}_{\text{leak}} = \sum_{\mu} d_{\mu}^{(+)} \mathcal{D}\left[\hat{Q}_{\mu}\right] \tag{20b}$$

where $\mathcal{D}[\hat{O}]\,\hat{\rho} = \hat{O}\hat{\rho}\hat{O}^{\dagger} - \frac{1}{2}\{\hat{O}^{\dagger}\hat{O}, \hat{\rho}\}$ for any operator $\hat{O}$. Diagonalizing the Hermitian Kossakowski matrix $\widetilde{W}$ only amounts to a rotation in the space of leakage operators, and the possible cross-damping encoded in the off-diagonal terms of $\widetilde{W}$ is not lost, but is absorbed into the jump operators $\hat{Q}_{\mu}$. This leads to the dissipator $\mathcal{L}_{\text{leak}}$, whose explicit form is $\sum_{j\mu} d_{\mu}^{(+)} \mathcal{D}[U_{j\mu}\hat{\sigma}_j]$ (with $d_{\mu} \to d_{\mu}^{(+)}$ because of the positivity projection, if needed). A detailed assessment of this procedure and its accuracy is given in [26].

3.2. UP–LP scattering and pure dephasing

Incoherent UP↔LP scattering processes are described by the jump operators

$$\hat{L}_{\downarrow} = \hat{B}_{-}^{\dagger}\hat{B}_{+}, \qquad \hat{L}_{\uparrow} = \hat{B}_{+}^{\dagger}\hat{B}_{-}, \tag{21}$$

with corresponding rates $\gamma_{\downarrow}$ and $\gamma_{\uparrow}$, respectively, which may be constrained by detailed-balance relation if the baths are thermal. In the zero-temperature numerical examples considered below, we set $\gamma_{\uparrow} = 0$ and retain $\gamma_{\downarrow}$ only as a weak phenomenological incoherent channel. Pure dephasing of each polariton branch is modeled by the number operators

$$\hat{L}_{\phi,+} = \hat{N}_{+}, \qquad \hat{L}_{\phi,-} = \hat{N}_{-}, \tag{22}$$

with dephasing rates $\gamma_{\phi,+}$ and $\gamma_{\phi,-}$, which we assume to be equal and denote as γ_{ϕ}.

3.3. Final form of the Lindbladian master equation

Collecting all contributions, the full driven dynamics of the hybrid cavity, including the coherent drives according to equation (7) and additional scattering and dephasing channels, is described by the non-secular master equation

$$\frac{\mathrm{d}\hat{\rho}}{\mathrm{d}t} = -\mathrm{i}\left[\hat{H}_{\text{s}} + \hat{H}_{\text{LS}} + \hat{H}_{\text{drive}}(t), \hat{\rho}\right] + \mathcal{L}_{\text{tot}}\,\hat{\rho}, \tag{23}$$

where

$$\begin{aligned}\mathcal{L}_{\text{tot}} &= \mathcal{L}_{\text{leak}} + \mathcal{L}_{\text{scatt}} + \mathcal{L}_{\phi} \\ &= \mathcal{L}_{\text{leak}} + \sum_{k=\downarrow,\uparrow} \gamma_k \mathcal{D}\left[\hat{L}_k\right] + \gamma_{\phi} \sum_{k=\pm} \mathcal{D}\left[\hat{N}_k\right]\end{aligned} \tag{24}$$

is the total dissipator. Here $\mathcal{L}_{\text{leak}}$, equation (20b), encodes the leakage due to the interactions with the bath (shortly, the bath leakage, i.e. mode absorption and radiative losses), while $\mathcal{L}_{\text{scatt}} = \sum_{k=\downarrow,\uparrow} \gamma_k \mathcal{D}[\hat{L}_k]$ and $\mathcal{L}_{\phi} = \gamma_{\phi} \sum_{k=\pm} \mathcal{D}[\hat{N}_k]$ describe UP↔LP scattering and pure dephasing, respectively.

Equations (23) and (24) provide an accurate Lindblad (GKSL) description of the leakage dynamics of the hybrid cavity: the generator is linear in $\hat{\rho}$ and defines a completely positive and trace-preserving dynamical map by construction of the Kossakowski matrix, retaining the non-secular character of the leakage dynamics through the Hermitian quadrature coupling $\hat{X}$. In particular, the off-diagonal elements of $\widetilde{W}_{+}$ remain nonzero whenever the corresponding Bohr frequencies are closer than the bath linewidth, so that different polariton transitions still interfere in the dissipator. This goes beyond the standard secular Lindblad treatment, where the Kossakowski matrix is diagonal in the Bohr-frequency basis and all such cross terms are discarded.

We emphasize that, among all dissipative channels, only the leakage term is modified by retaining non-secular contributions: the Hermitian jump operator $\hat{X}$ generates cross-terms with oscillating factors at frequencies $\pm(\omega_{+} \pm \omega_{-})$, which can be discarded in the secular approximation. By contrast, the other dissipative channels considered do not contain similar cross-terms.

For the numerical implementation, it is convenient to use the standard column-stacking vectorization of the density matrix and the associated matrix representation of Lindblad superoperators [21, 42–45]. The following relations are included only to fix notation. We stack the columns of $\hat{\rho}(t)$ into a single d^2-component vector, $\text{vec}(\hat{\rho}(t))$, via the map $\text{vec}: \mathbb{C}^{d\times d} \to \mathbb{C}^{d^2}$. Using the standard identity

$$\text{vec}\left(\hat{A}\hat{\rho}\hat{B}\right) = \left(\hat{B}\,T \otimes \hat{A}\right) \text{vec}\left(\hat{\rho}\right), \tag{25}$$

valid for arbitrary operators $\hat{A}$ and $\hat{B}$, equation (23) can be written as

$$\frac{\mathrm{dvec}\,(\hat{\rho})}{\mathrm{d}t} = \mathbf{L}\,(t)\,\mathrm{vec}\,(\hat{\rho}) = (\mathbf{L}_H\,(t)\ + \mathbf{L}_{\mathrm{diss}})\,\mathrm{vec}\,(\hat{\rho})\,, \tag{26}$$

where $\mathbf{L}(t)$ is the total $d^2 \times d^2$ Liouvillian matrix. The Hamiltonian contribution $-\mathrm{i}[\hat{H}_{\mathrm{eff}}(t), \hat{\rho}]$, with $\hat{H}_{\mathrm{eff}}(t) = \hat{H}_{\mathrm{s}} + \hat{H}_{\mathrm{LS}} + \hat{H}_{\mathrm{drive}}(t)$, yields

$$\mathbf{L}_H\,(t) = -\mathrm{i}\left(\mathbb{I}_d \otimes \hat{H}_{\mathrm{eff}}\,(t) - \hat{H}_{\mathrm{eff}} T\,(t) \otimes \mathbb{I}_d\right), \tag{27}$$

while $\mathbf{L}_{\mathrm{diss}} = \sum_i \mathbf{L}_{\hat{\mathcal{J}}_i}$ is the matrix representation of the total dissipator in equation (24), with each jump operator $\hat{\mathcal{J}}_i \in \{\hat{Q}_\mu, \hat{L}_\uparrow, \hat{L}_\downarrow, \hat{N}_+, \hat{N}_-\}$ contributing through the standard superoperator form

$$\mathbf{L}_{\hat{\mathcal{J}}_i} = \hat{\mathcal{J}}_i^* \otimes \hat{\mathcal{J}}_i - \frac{1}{2}\mathbb{I}_d \otimes \left(\hat{\mathcal{J}}_i^\dagger \hat{\mathcal{J}}_i\right) - \frac{1}{2}\left(\hat{\mathcal{J}}_i^\dagger \hat{\mathcal{J}}_i\right) T \otimes \mathbb{I}_d. \tag{28}$$

These standard relations define the closed system of d^2 first-order linear differential equations that we integrate numerically below.

4. The dynamics of bright and dark polaritons

The QME (23) provides a natural starting point for comparing the leakage dynamics predicted by the full, non-secular description and its secular approximation. It is especially illuminating to reorganize the UP/LP polariton branches into *bright* and *dark* superpositions, which clarify the structure of the system–bath coupling.

The bright and dark single-excitation states are defined in the one-excitation subspace $\mathrm{span}\{|0,1\rangle, |1,0\rangle\}$ as

$$|\mathrm{b}\rangle = \frac{|1,0\rangle + |0,1\rangle}{\sqrt{2}}, \qquad |\mathrm{d}\rangle = \frac{|1,0\rangle - |0,1\rangle}{\sqrt{2}}, \tag{29}$$

and they are annihilated by the corresponding mode operators

$$\hat{B}_{\mathrm{b}} = \frac{\hat{B}_+ + \hat{B}_-}{\sqrt{2}}, \qquad \hat{B}_{\mathrm{d}} = \frac{\hat{B}_+ - \hat{B}_-}{\sqrt{2}}. \tag{30}$$

Because the truncation includes the double-excitation state $|1,1\rangle$, the number operators $\hat{N}_{\mathrm{b,d}} = \hat{B}_{\mathrm{b,d}}^\dagger \hat{B}_{\mathrm{b,d}}$ receive contributions from both the single-excitation manifold and the $|1,1\rangle$ sector. To quantify the bright and dark populations, we therefore use the projectors

$$\hat{P}_{\mathrm{b}} = |\mathrm{b}\rangle\langle\mathrm{b}|\,, \qquad \hat{P}_{\mathrm{d}} = |\mathrm{d}\rangle\langle\mathrm{d}|\,, \tag{31}$$

whose expectation values $\langle \hat{P}_{\mathrm{b,d}}(t)\rangle = \mathrm{Tr}[\hat{P}_{\mathrm{b,d}}\hat{\rho}(t)]$ are dimensionless probabilities in $[0,1]$. We also monitor the UP–LP coherence in the single-excitation manifold,

$$|\rho_{\mathrm{c}}\,(t)\,| = |\langle 1,0|\hat{\rho}\,(t)\,|0,1\rangle|, \tag{32}$$

since the non-secular damping cross-terms act precisely through these coherences. The transition operators

$$\begin{aligned} \hat{\sigma}_1 &\equiv \hat{B}_+ = |0,0\rangle\,\langle 1,0| + |0,1\rangle\,\langle 1,1|\,, \\ \hat{\sigma}_2 &\equiv \hat{B}_- = |0,0\rangle\,\langle 0,1| + |1,0\rangle\,\langle 1,1|\,, \end{aligned} \tag{33}$$

collect the two degenerate lowering transitions at Bohr frequencies $\omega_1 \simeq \omega_+$ and $\omega_2 \simeq \omega_-$, respectively (strict equality is usually assumed, neglecting the small shifts due to coherent mixing and bath-induced renormalization when evaluating the rates). In contrast, the bright and dark single-excitation states $|\mathrm{b}\rangle$ and $|\mathrm{d}\rangle$ are superpositions of eigenstates with different Bohr frequencies; consequently, the transitions from $|\mathrm{b}\rangle$ and $|\mathrm{d}\rangle$ to the vacuum are not associated with a unique frequency, but involve both ω_+ and ω_-.

In the numerical calculations, we use truncated polariton Fock spaces of the form $0 \leqslant n_\pm \leqslant N_{\max}$, with the cutoff chosen according to the purpose of the calculation. The minimal truncation, $N_{\max} = 1$, is useful for isolating the single-excitation bright and dark leakage physics in the most transparent way, but

it is not assumed a priori to remain quantitatively accurate once coherent driving begins to populate higher-excitation sectors. For $N_{\max} > 1$, the dynamics is evolved in the enlarged Hilbert space, while the monitored observables are still defined with respect to the single-excitation sector, namely the projectors $\hat{P}_{\rm b}$ and $\hat{P}_{\rm d}$ and the coherence $|\rho_{\rm c}(t)|$. In contrast, the explicit 4-level component equations in appendix B and the associated closed-form steady-state formulas in appendix C refer, for simplicity, to the minimal truncation $N_{\max} = 1$.

4.1. Breakdown of the secular approximation

According to equations (14) and (16), the diagonal elements $W_{11}(\omega_1)$ and $W_{22}(\omega_2)$ are given by $J(\omega_1)$ and $J(\omega_2)$, respectively, while the off-diagonal effective dissipative terms are

$$\widetilde{W}_{12} = \sqrt{W_{12}(\omega_1)\, W_{12}(\omega_2)} = \sqrt{J(\omega_1)\, J(\omega_2)}. \tag{34}$$

For a Lorentzian $J(\omega)$ of width $\gamma_{\rm D}$ centered near the plasmonic resonance, this expression yields two distinct regimes:

- If $|\Delta| \lesssim \gamma_{\rm D}/2$, then $J(\omega_1) \simeq J(\omega_2)$ and equation (34) implies $\widetilde{W}_{12} \sim W_{11} \sim W_{22}$. In this unresolved regime, the two transitions are effectively coupled by the same reservoir, so cross-damping and interference cannot be neglected: the dissipation eigenchannels become collective bright and dark modes, the bath-induced coherence is non-negligible, and a comparatively long-lived dark mode may emerge. Therefore the full non-secular leakage kernel in $\mathcal{L}_{\rm tot}$ must be retained. In the numerical implementation, for the two leakage channels $\hat{\sigma}_1 \equiv \hat{B}_+$ and $\hat{\sigma}_2 \equiv \hat{B}_-$, the geometrically averaged dissipative kernel entering the non-secular leakage term is taken as [46]

$$\widetilde{W} = \begin{pmatrix} J(\omega_+) & g \\ g & J(\omega_-) \end{pmatrix}, \qquad \kappa_{\rm c} = \frac{(\gamma_{\rm D}/2)^2}{(\gamma_{\rm D}/2)^2 + \Delta^2}, \qquad g = \kappa_{\rm c}\sqrt{J(\omega_+)J(\omega_-)}, \tag{35}$$

  where $\kappa_{\rm c}$ quantifies the suppression of cross-damping by finite bath memory, so that $\kappa_{\rm c} \to 1$ for $\Delta \ll \gamma_{\rm D}/2$ (unresolved transitions) and $\kappa_{\rm c} \to 0$ for $\Delta \gg \gamma_{\rm D}/2$.

  We call this *common-bath* regime, because the bath correlation time $\gamma_{\rm D}$ is long enough that the bath cannot distinguish the $\omega_\pm$ transitions, so they effectively couple to the same reservoir mode continuum and acquire appreciable cross damping g.

  The Hermitian matrix $\widetilde{W}$ is then diagonalized as $\widetilde{W} = U\,\mathrm{diag}(d_\mu)\,U^\dagger$ and, if needed, projected onto its positive part by setting $d_\mu^{(+)} = \max(d_\mu, 0)$, where

$$d_\pm = \frac{J(\omega_+) + J(\omega_-)}{2} \pm \sqrt{\left(\frac{J(\omega_+) - J(\omega_-)}{2}\right)^2 + g^2}. \tag{36}$$

  This yields a GKSL-form dissipator with non-negative rates. For the 2×2 kernel in equation (35) one may write $\widetilde{W} = U\,\mathrm{diag}(d_+, d_-)\,U^\dagger$ with a rotation $U(\theta)$ defined by $\tan(2\theta) = 2g/[J(\omega_+) - J(\omega_-)]$, so that the jump operators are linear combinations of the original transitions, $\hat{Q}_+ = \cos\theta\,\hat{\sigma}_1 + \sin\theta\,\hat{\sigma}_2$ and $\hat{Q}_- = -\sin\theta\,\hat{\sigma}_1 + \cos\theta\,\hat{\sigma}_2$. Thus, the off-diagonal coefficient $g = \widetilde{W}_{12}$ is absorbed into the structure of $\hat{Q}_\pm$ (and into the eigenvalues $d_\pm$), rather than being discarded. The resulting generator is of GKSL form and therefore defines completely positive and trace-preserving reduced dynamics.
  In the symmetric case $J(\omega_+) = J(\omega_-) \equiv \Gamma$, one has $d_\pm = \Gamma \pm g = \Gamma(1 \pm \kappa_{\rm c})$, and the jump operators reduce to the bright and dark superpositions $\hat{Q}_\pm \propto \hat{B}_+ \pm \hat{B}_-$ (Hadamard rotation).

- If $|\Delta| \gg \gamma_{\rm D}$, the bath resolves the two transition frequencies on its correlation-time scale and the oscillatory cross terms average out. Accordingly, the off-diagonal coefficients are strongly suppressed, $\widetilde{W}_{12} \ll W_{11}, W_{22}$, and the leakage is well described by independent decay channels governed by $J(\omega_1)$ and $J(\omega_2)$. In this resolved regime the secular approximation is justified and the secular and non-secular generators yield practically identical dynamics [47]. The leakage dynamics are well described by a dissipator of the form

$$\mathcal{L}_{\rm leak}^{(\rm sec)}\hat{\rho} \simeq \sum_{k=\pm} \Gamma_k \left(\hat{B}_k \hat{\rho} \hat{B}_k^\dagger - \tfrac{1}{2}\left\{\hat{B}_k^\dagger \hat{B}_k, \hat{\rho}\right\}\right), \tag{37}$$

with decay rates Γ_k obtained from $J(\omega_k)$ via the microscopic self-energy $\mathcal{S}(\omega_k)$. It is important to emphasize that the QME equations (23) and (24) retains the non-secular couplings while guaranteeing complete positivity, whereas a fully secular Lindblad equation based on independent decay channels often predicts much faster decay of dark excitations and substantially different steady-state populations.

In this approach, the separation Δ is determined by the light–matter coupling strength $\xi\Omega_{\rm pl}$ and the losses $\gamma_{\rm D}$, as described in section 2 and appendix A, equation (A2). Our microscopic construction thus establishes a direct connection between the internal EC–SPP hybridization physics, which sets the UP–LP splitting, and the validity of the secular approximation for the leakage dynamics, governed by the ratio $\Delta/\gamma_{\rm D}$. Notably, the regime where non-secular effects become relevant does not, in principle, require ultrastrong coupling: even for moderate splittings, secular breakdown can occur whenever Δ is comparable to the bath linewidth. Conversely, in the ultrastrong-coupling regime, the larger separation can push the system toward the secular limit, provided that Δ exceeds the Drude–Lorentz width. The numerical values used below should therefore be understood as physically motivated benchmark parameters illustrating this crossover in lossy EC–SPP systems, rather than as a quantitative fit to a specific experiment.

A distinctive feature of the common-bath regime is the possible emergence of an interference-protected dark polaritonic combination. In the present model, this is a linear dissipative effect selected by the common leakage channel, not a nonlinear-emitter dark state. Its relevance lies in loss redistribution, suppression of radiative decay, and the emergence of a comparatively longer-lived polaritonic component. Importantly, this mechanism is controlled by the unresolved-transition condition $\Delta \lesssim \gamma_{\rm D}$ and does not, in principle, require ultrastrong coupling.

We do not mean that the present EC–SPP model realizes exactly the same physical setting as [28–30]. Rather, these references are cited only to indicate that dark-state polaritons and related interference-protected modes are a broader phenomenon in driven-dissipative bosonic systems, while [30] provides experimental evidence in a more directly polaritonic solid-state platform. In the present model, the relevant dark mode is the bath-induced bright/dark superposition selected by the common leakage channel. Specifically, when $\Delta \simeq \gamma_{\rm D}$, the Kossakowski matrix associated with the leakage channel has a bright eigenmode proportional to $(\sigma_+ + \sigma_-)$ with a finite eigenvalue, and an orthogonal dark eigenmode proportional to $(\sigma_+ - \sigma_-)$ with a numerically vanishing eigenvalue. Consequently, the corresponding jump operators act only on the bright superposition $\hat{B}_{\rm b}$, while the dark superposition $\hat{B}_{\rm d}$ does not couple directly to the common bath and is ideally protected within the leakage-only approximation considered here. When incoherent UP↔LP scattering and pure dephasing channels are included, this exact protection is lost: these additional processes do not preserve the bright/dark decomposition and introduce leakage pathways for $\hat{B}_{\rm d}$, turning the dark polariton into a *quasi*-protected mode with a finite yet parametrically longer lifetime than the bright one.

4.2. Numerical comparison of secular and non-secular dynamics

To explicitly compare the dynamics obtained from the full non-secular master equation and its secular approximation, we numerically integrate the time-local GKSL master equation in the considered truncated polariton Fock space, so the Liouvillian superoperator acts on a $d^2 = 16$-dimensional vectorized density matrix. A convenient ordered basis is $|1\rangle = |0,0\rangle$, $|2\rangle = |0,1\rangle$, $|3\rangle = |1,0\rangle$, $|4\rangle = |1,1\rangle$. The vectorized form of the density matrix is

$$\mathrm{vec}\,(\hat{\rho}) = \left(\rho_{11},\ \rho_{21},\ \rho_{31},\ \rho_{41},\ \rho_{12},\ \ldots,\ \rho_{44}\right)^T, \tag{38}$$

where the columns of $\hat{\rho}$ are stacked into a single column vector of length $d^2 = 16$.

The single-mode annihilation operator in the truncated basis $\{|0\rangle, |1\rangle\}$ is

$$\hat{b} = \begin{pmatrix} 0 & 1 \\ 0 & 0 \end{pmatrix}, \tag{39}$$

and the polariton annihilation operators $\hat{B}_\pm$ are built as

$$\hat{B}_+ = \hat{b} \otimes \mathbb{I}_2, \qquad \hat{B}_- = \mathbb{I}_2 \otimes \hat{b}, \tag{40}$$

which yield explicitly

$$\hat{B}_+ = \begin{pmatrix} 0 & 0 & 1 & 0 \\ 0 & 0 & 0 & 1 \\ 0 & 0 & 0 & 0 \\ 0 & 0 & 0 & 0 \end{pmatrix}, \qquad \hat{B}_- = \begin{pmatrix} 0 & 1 & 0 & 0 \\ 0 & 0 & 0 & 0 \\ 0 & 0 & 0 & 1 \\ 0 & 0 & 0 & 0 \end{pmatrix}. \tag{41}$$

We consider a two-stage driving protocol designed to prepare and probe the bright/dark structure of the leakage dynamics. The non-secular effect originates from the common-bath dissipator and does not, in principle, require any Raman-like coupling. The two coherent controls used here serve a diagnostic purpose: the stage-1 bright drive prepares a population in the symmetric combination, while the stage-2 dark drive, together with the Raman-like UP–LP coupling, mixes the bright and dark sectors and enhances the contrast between secular and non-secular leakage in the monitored observables.

Starting from an initial vacuum state $\hat{\rho}(0) = |0,0\rangle\langle 0,0|$, a coherent drive with amplitude f and frequency ω_c is switched on at $t = 0$ and illuminates the cavity for $0 \leqslant t < t_{sw}$ (stage-1), which populates the symmetric (bright) superposition of upper and lower polaritons,

$$\hat{H}^{(b)}_{drive} = f\left(\hat{B}_+ + \hat{B}_- + \hat{B}^\dagger_+ + \hat{B}^\dagger_-\right), \qquad 0 \leqslant t < t_{sw}. \tag{42}$$

In this regime the Raman-like UP–LP coupling is switched off. At $t = t_{sw}$ (stage-2) we turn on a coherent interbranch (Raman-like) coupling of strength $\mathcal{R}_{UPLP}$,

$$\hat{H}_R = \mathcal{R}_{UPLP}\left(\hat{B}^\dagger_+\hat{B}_- + \hat{B}^\dagger_-\hat{B}_+\right), \qquad t_{sw} \leqslant t < t_{off}, \tag{43}$$

and change the illumination pattern to a *dark* drive that populates the antisymmetric superposition,

$$\hat{H}^{(d)}_{drive} = f\left(\hat{B}_+ - \hat{B}_- + \hat{B}^\dagger_+ - \hat{B}^\dagger_-\right). \tag{44}$$

For $t \geqslant t_{off}$, the coherent drives and the Raman coupling are switched off, and the system evolves freely under leakage, scattering, and dephasing.

While equations (26)–(28) provide a compact vectorized form useful for discussion, for numerical integration it is necessary to write the corresponding system of coupled first-order ODEs for the density-matrix elements explicitly in the truncated polariton Fock space $n_\pm \leqslant 1$. The derivation is given in appendix B, which provides the time evolution of the bright and dark projectors, $\langle \hat{P}_b(t)\rangle$ and $\langle \hat{P}_d(t)\rangle$.

To highlight the role of the UP–LP frequency separation Δ relative to the bath linewidth, in figure 2 we compare the results obtained for two cases: a regime with $\Delta = 0.015\,\mathrm{ps}^{-1} \lesssim \gamma_D$ and a well-resolved regime $\Delta = 0.15\,\mathrm{ps}^{-1} \gg \gamma_D$. The numerical parameters used are: bath linewidth (correlation rate) $\gamma_D = 0.04\,\mathrm{ps}^{-1}$, central frequency $\omega_c = 1\,\mathrm{ps}^{-1}$, zero-temperature leakage bath, scattering rate $\gamma_\downarrow = 10^{-3}\,\mathrm{ps}^{-1}$, $\gamma_\uparrow = 0$, and pure dephasing $\gamma_\phi = 5 \times 10^{-4}\,\mathrm{ps}^{-1}$. The latter two channels are included only as weak phenomenological perturbations. The coherent drive amplitude f and the Raman-like coupling strength $\mathcal{R}_{UPLP}$ are $0.01\,\mathrm{ps}^{-1}$; we take $t_{sw} = 1000\,\mathrm{ps}$, $t_{off} = 3000\,\mathrm{ps}$, and integrate up to $t_{max} = 4000\,\mathrm{ps}$.

The values of $\gamma_\downarrow$ and γ_ϕ used in the numerical examples are not intended as a quantitative fit to any specific experiment, but rather serve as weak phenomenological perturbations introduced to test the robustness of the non-secular leakage effect. This is a controlled limit, as experimentally reported polariton relaxation and broadening processes are often much faster, typically occurring on sub-picosecond to tens of picoseconds timescales. In many experimental studies [48, 49], pure dephasing is not introduced explicitly but is instead incorporated into effective linewidths or reservoir-assisted relaxation. Here, however, an explicit γ_ϕ is useful because the central effect is coherence-sensitive and relies on interference between unresolved UP and LP leakage pathways.

To assess whether the single-excitation description remains valid in the presence of coherent driving, we monitored both the occupation of the highest retained state and, for larger cutoffs, the population escaping the minimal subspace $\{0 \leqslant n_\pm \leqslant 1\}$. For the representative weak-drive benchmark point considered here ($\Delta = 0.015\ \mathrm{ps}^{-1}$, $\gamma_D = 0.04\ \mathrm{ps}^{-1}$, $f = 0.01\ \mathrm{ps}^{-1}$), simulations with $N_{max} = 2$ and 3 show quantitative stability in the observables of interest: during stage 2, the differences between the $N_{max} = 2$ and $N_{max} = 3$ results remain below 2.1×10^{-3} for $\langle \hat{P}_b\rangle$, below 7.2×10^{-3} for $\langle \hat{P}_d\rangle$, and below 3.8×10^{-3} for $|\rho_c|$. This indicates that the weak-drive benchmark is converged at the relevant level, although the minimal truncation $N_{max} = 1$ can still produce noticeable quantitative shifts, especially in $\langle \hat{P}_d\rangle$ and $|\rho_c|$. Accordingly, figure 2 is presented with $N_{max} = 2$. In contrast, for stronger driving, representative convergence tests with increased cutoffs show that the dynamics explores significantly higher excitation sectors and converges slowly with N_{max}. Specifically, even at the benchmark point

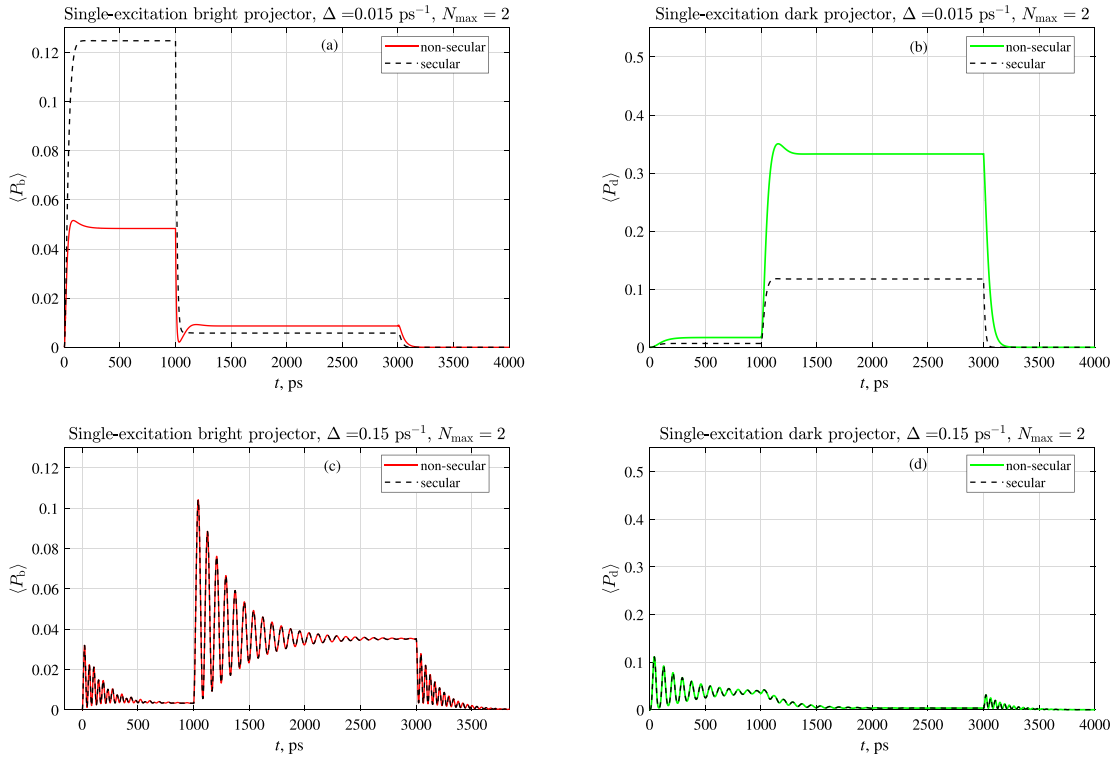

Figure 2. Time evolution under the two-stage drive protocol of the single-excitation bright and dark populations, $\langle \hat{P}_{\rm b}(t)\rangle$ and $\langle \hat{P}_{\rm d}(t)\rangle$. Solid lines: full non-secular common-bath leakage; dashed lines: secular approximation (diagonal Kossakowski matrix). Parameters: leakage bath in the zero-temperature limit, $\gamma_{\rm D} = 0.04$ ps^{-1}, $\Gamma_{\rm pl} = 2\gamma_{\rm D}$, $\gamma_{\downarrow} = 10^{-3}$ ps^{-1}, $\gamma_{\uparrow} = 0$, $\gamma_{\phi} = 5\times 10^{-4}$ ps^{-1}, and drive amplitude $f = 0.01$ ps^{-1}. The bright drive is applied for $0 \leqslant t < t_{\rm sw}$ with $t_{\rm sw} = 1000$ ps, while for $t_{\rm sw} \leqslant t < t_{\rm off}$ (with $t_{\rm off} = 3000$ ps) the illumination switches to the dark drive and a Raman-like coupling $R_{\rm UP-LP} = 0.01$ ps^{-1} is turned on. Panels (a), (b): $\Delta = 0.015$ ps^{-1}; panels (c), (d): $\Delta = 0.15$ ps^{-1}. The dynamics are computed with the enlarged cutoff $N_{\max} = 2$, while the plotted observables remain the single-excitation projectors and coherence defined in the $\{|0,1\rangle, |1,0\rangle\}$ manifold.

$(\Delta, \gamma_D) = (0.015, 0.04)$ ps^{-1}, the population in the highest retained shell remains substantial at large cutoffs. Therefore, the stronger-drive scan discussed in section 4.3 should be viewed primarily as a qualitative illustration of the crossover trend, rather than as a quantitatively converged map.

In the first case figures 2(a) and (b), the leakage bath cannot resolve the UP and LP frequencies, so the geometric-mean cross rates in the Kossakowski matrix $\widetilde{W}_{12}$ remain significant, and the non-secular dynamics produces visible deviations from the secular approximation, most clearly in the build-up and decay of the dark-state population. In contrast, for $\Delta \gg \gamma_{\rm D}$ figures 2(c) and (d), the secular and non-secular leakage models become practically indistinguishable throughout the driven dynamics, due to the suppression of the effective cross rates $\widetilde{W}_{12}$.

Approximate steady-state solutions for $\langle \hat{P}_{\rm b,d}\rangle$ can be obtained by setting the derivative in equations (26)–(28) to zero. The procedure is described in detail in appendix C, neglecting the Raman-like coupling and UP–LP scattering. In the secular approximation, this yields the following expressions ('ss' for steady state and 'sec' for secular):

$$\begin{aligned}\langle \hat{P}_{\rm b}\rangle_{\rm ss}^{(\rm sec)}\big|_{\rm bright\ drive} &= \frac{4f^2}{D^2}\left(2\Gamma^2 + 4f^2\right),\\ \langle \hat{P}_{\rm d}\rangle_{\rm ss}^{(\rm sec)}\big|_{\rm bright\ drive} &= \frac{4f^2}{D^2}\left(2\Delta^2 + 4f^2\right),\end{aligned} \tag{45}$$

for the bright drive, while for the dark drive the two expressions are exchanged,

$$\begin{aligned}\langle \hat{P}_{\rm b}\rangle_{\rm ss}^{(\rm sec)}\big|_{\rm dark\ drive} &= \langle \hat{P}_{\rm d}\rangle_{\rm ss}^{(\rm sec)}\big|_{\rm bright\ drive}\\ \langle \hat{P}_{\rm d}\rangle_{\rm ss}^{(\rm sec)}\big|_{\rm dark\ drive} &= \langle \hat{P}_{\rm b}\rangle_{\rm ss}^{(\rm sec)}\big|_{\rm bright\ drive}.\end{aligned} \tag{46}$$

where Γ is given by equation (11), and $D = \Gamma^2 + \Delta^2 + 8f^2$.

When the non-secular terms are retained, the presence of the cross-damping terms requires a different approach, also described in appendix C. For the two drives, the steady-state solutions for $\langle \hat{P}_{\rm b,d}\rangle$ are

Table 1. Stationary solutions, $\Delta = 0.015\,\mathrm{ps}^{-1}$.

	$\langle\hat{P}_\mathrm{b}\rangle_\mathrm{ss}^{(\mathrm{ns})}$	$\langle\hat{P}_\mathrm{b}\rangle_\mathrm{ss}^{(\mathrm{sec})}$	$\langle\hat{P}_\mathrm{d}\rangle_\mathrm{ss}^{(\mathrm{ns})}$	$\langle\hat{P}_\mathrm{d}\rangle_\mathrm{ss}^{(\mathrm{sec})}$
bright drive	0.056	0.116	2.17×10^{-3}	9.6×10^{-3}
dark drive	0.014	9.6×10^{-3}	0.352	0.116

('ns' standing for non-secular)

$$\langle\hat{P}_\mathrm{b}\rangle_\mathrm{ss}^{(\mathrm{ns})}\big|_{\text{bright drive}} = \frac{32f^2\left[\Gamma^2+2f^2\right]}{\mathcal{N}_\mathrm{b}},$$
$$\langle\hat{P}_\mathrm{d}\rangle_\mathrm{ss}^{(\mathrm{ns})}\big|_{\text{bright drive}} = \frac{64f^4}{\mathcal{N}_\mathrm{b}} \tag{47}$$
$$\langle\hat{P}_\mathrm{b}\rangle_\mathrm{ss}^{(\mathrm{ns})}\big|_{\text{dark drive}} = \frac{64f^4}{\mathcal{N}_\mathrm{b}},$$
$$\langle\hat{P}_\mathrm{d}\rangle_\mathrm{ss}^{(\mathrm{ns})}\big|_{\text{dark drive}} = \frac{32f^2\left[\Gamma^2+2f^2\right]}{\mathcal{N}_\mathrm{d}}, \tag{48}$$

where $\mathcal{N}_{\mathrm{b,d}} = 4\Gamma^2\left(\Gamma_{\mathrm{b,d}}^2+16f^2\right)+(4f)^4$.

With parameters as in figure 2 and $\Delta = 0.015$, the steady state values provided by equations (45) – (48) are shown in table 1, which are in good agreement with figure 2.

For $|\Delta| \gg \gamma_\mathrm{D}/2$ (so that $\kappa_\mathrm{c}\to 0$), the cross-correlations are suppressed ($g\to 0$), and the natural jump operators approach $\hat{B}_\pm$ instead. As described in detail in appendix C, the bright and dark ladder solutions given by equations (47) and (48) are no longer representative, whereas the component rate equations and the numerical GKSL integration results (e.g. figure 2, as well as figures 3 and 4 described in section 4.3) remain valid for arbitrary Δ.

4.3. Parameter space investigation

To identify the parameter region where non-secular leakage terms are quantitatively relevant and to provide design guidance, we perform a two-dimensional scan over the polariton splitting Δ and the Drude–Lorentz linewidth γ_D, comparing the non-secular common-bath dynamics with its secular approximation under the same two-stage protocol as in figure 2. Since the interference-driven signatures (bath-induced coherence and bright-dark selectivity) are most clearly revealed during the second stage, where the dark drive is combined with a Raman-like UP–LP mixing term, we quantify discrepancies by the stage-2 maximum deviation,

$$D_\mathrm{max}^{(X)}(\Delta,\gamma_\mathrm{D}) = \max_{t\in[t_\mathrm{sw},t_\mathrm{off}]}\left|X_\mathrm{ns}(t)-X_\mathrm{sec}(t)\right|, \tag{49}$$

with $X\in\{\langle\hat{P}_\mathrm{b}\rangle,\langle\hat{P}_\mathrm{d}\rangle,|\rho_\mathrm{c}|\}$. The results are shown as color maps in figure 3 for weak coherent couplings and in figure 4 for stronger driving, in the $(\Delta,\gamma_\mathrm{D})$ parameter space. As for figure 2, the dynamics is computed with the enlarged cutoff $N_\mathrm{max}=2$.

For both drive strengths, the largest deviations occur in the 'unresolved' regime $\Delta\lesssim\gamma_\mathrm{D}$, where the reservoir cannot distinguish the UP and LP transition frequencies on the bath-correlation scale and the cross-damping terms in the common-bath kernel are not averaged out. For $\Delta\gg\gamma_\mathrm{D}$ the discrepancies rapidly collapse, consistent with the suppression of off-diagonal dissipative couplings.

In the weak-drive case (figure 3), two distinct features appear at small Δ. First, a localized enhancement of $D_\mathrm{max}^{(\langle\hat{P}_\mathrm{b}\rangle)}$ at small Δ and small γ_D originates from the bright population prepared during stage 1: when the leakage rate is slow on the stage-2 time window, a residual bright component survives the switching and enters stage 2, so the non-secular correction to the effective bright decay channel yields a visible mismatch in $\langle\hat{P}_\mathrm{b}\rangle$. Second, for larger γ_D at the same small Δ, dissipation acts on the stage-2 timescale and the dominant difference becomes the fate of the dark combination: the secular approximation predicts independent decay governed by $J(\omega_\pm)$, whereas the non-secular common-bath kernel approaches a nearly rank-one form and partially protects the orthogonal dark state through destructive interference. This produces the vertical high-deviation region in $D_\mathrm{max}^{(\langle\hat{P}_\mathrm{d}\rangle)}$ and the concomitant enhancement of $D_\mathrm{max}^{(|\rho_\mathrm{c}|)}$ at small Δ.

In the strong-drive case (figure 4), the crossover between secular and non-secular behavior is still determined by the ratio Δ/γ_D, but the deviations are spread over a broader upper-left wedge. Compared to the weak-drive scan, the stage-2 discrepancies are generally reduced because the stronger dark drive

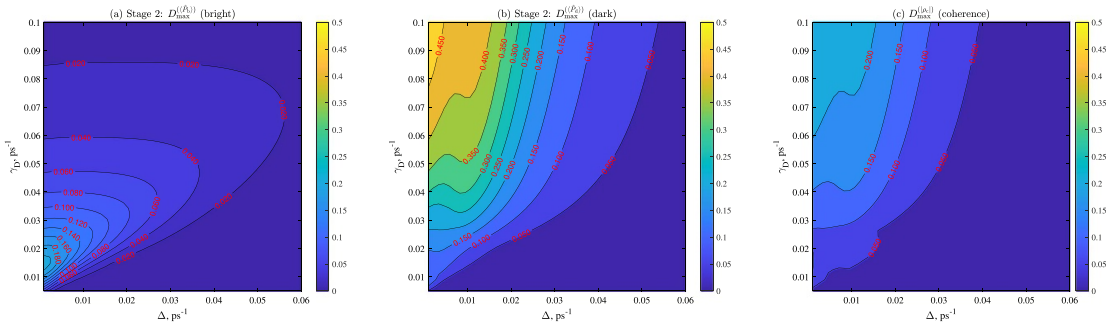

Figure 3. Stage-2 maximum deviation $D_{\max}^{(X)}(\Delta, \gamma_D)$, equation (49), between the non-secular common-bath leakage model and its secular approximation, for $X = \langle\hat{P}_b\rangle$ (a), $\langle\hat{P}_d\rangle$ (b), and $|\rho_c|$ (c), evaluated over the stage-2 time window of figure 2 while scanning Δ and γ_D. The bath spectrum is Lorentzian, equation (10), with FWHM γ_D and peak rate $\Gamma_{pl} \equiv J(\omega_{pl}) = 2\gamma_D$. Weak coherent couplings: $f = \mathcal{R}_{UP-LP} = 0.01$ ps^{-1}. The dynamics is computed with the enlarged cutoff $N_{\max} = 2$, while the plotted observables remain the single-excitation projectors and coherence defined in the $\{|0,1\rangle, |1,0\rangle\}$ manifold.

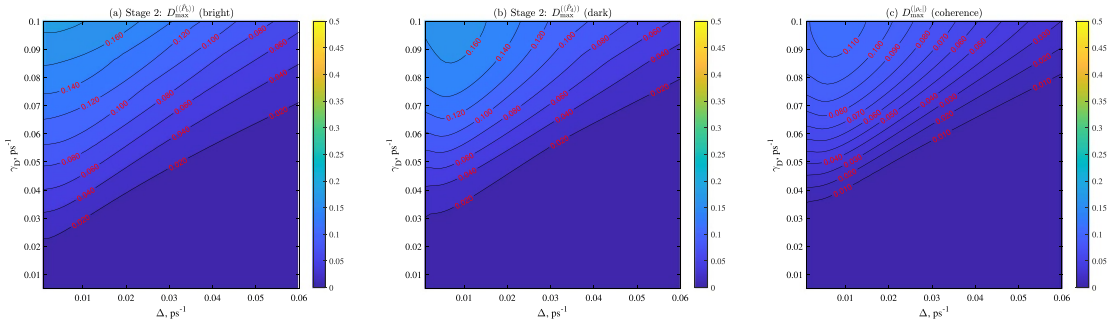

Figure 4. Same as figure 3, but for larger coherent amplitudes $f = \mathcal{R}_{UP-LP} = 0.1$ ps^{-1} within the same system–bath master-equation treatment, shown as a qualitative strong-drive illustration.

and Raman coupling transiently populate higher-lying states (including $|1,1\rangle$). This lowers the instantaneous weight of the single-excitation projectors during stage 2 and reduces their absolute mismatches. In this regime, $D_{\max}^{(\langle\hat{P}_d\rangle)}$ remains the most sensitive indicator, while $D_{\max}^{(\langle\hat{P}_b\rangle)}$ and $D_{\max}^{(|\rho_c|)}$ follow similar contours with smaller amplitudes.

5. Conclusions and outlook

We developed a Markovian master-equation framework for leakage in a hybrid plasmonic cavity beyond the secular approximation, based on the Drude–Lorentz response of the medium and the associated photon self-energy $\mathcal{S}(\omega)$. The resulting time-local generator preserves off-diagonal BR couplings between transitions at different Bohr frequencies and is completely positive.

In the bright/dark basis, the physical meaning of the non-secular leakage channel is clear. For a single-peaked Drude–Lorentz spectral density with width γ_D, cross-damping scales as $\sqrt{J(\omega_+)J(\omega_-)}$ and becomes significant when the polariton splitting satisfies $\Delta \lesssim \gamma_D$. In this regime, the two decay paths interfere and bath-induced coherences are generated: leakage acts mainly on the bright combination, while the orthogonal dark combination can become comparatively long-lived due to destructive interference. In the present linear bosonic setting, this is relevant for linewidth control and selective suppression of radiative leakage, rather than for nonlinear-emitter dark-state applications.

Numerical simulations in the truncated polariton Fock space with $n_+, n_- \leqslant 1$ make these regimes explicit. By monitoring the single-excitation bright and dark projectors and the UP–LP coherence under a two-stage bright/dark drive protocol, we find that non-secular leakage can sustain dark-state population and bath-induced coherence, whereas the secular approximation can overestimate dark decay and suppress coherence when $\Delta \sim \gamma_D$. For $\Delta \gg \gamma_D$, the non-secular generator smoothly approaches the secular limit, and the two descriptions become essentially indistinguishable.

Beyond clarifying open-system physics, these results highlight experimentally relevant functionalities. In particular, the non-secular regime enables linewidth engineering, selective enhancement or suppression of radiative leakage, and preparation of a longer-lived dark polaritonic component sustained by destructive interference in the leakage channel. Because the crossover is controlled by the single ratio Δ/γ_D, the framework provides a practical design rule for determining when a secular description is expected to fail.

The predicted effect can be tested experimentally using time-resolved transmission, reflectivity, or photoluminescence measurements while tuning the UP–LP splitting across the crossover from the resolved regime $\Delta \gg \gamma_D$ to the unresolved regime $\Delta \lesssim \gamma_D$. Observable signatures include redistribution of decay between bright and dark channels, longer-lived dark-state populations, and non-negligible UP–LP coherence in the common-bath regime. In hybrid plasmonic cavities, such tuning can be achieved by changing the cavity detuning, the effective EC–SPP coupling strength, or the metasurface geometry.

This framework provides a practical route to connect microscopic material response, Green's-function electrodynamics, and completely positive open-system dynamics in plasmonic cavity QED. Natural extensions include larger Fock-space truncations, multiple structured reservoirs (e.g. separating radiative and absorptive channels), inclusion of output fields to access emission spectra and correlation functions, and benchmarks against explicitly non-Markovian treatments when bath memory becomes comparable to system timescales.

Acknowledgments

This work was supported in part by the European Union under two initiatives of the Italian National Recovery and Resilience Plan (NRRP) of NextGenerationEU: the partnership on Telecommunications of the Future (PE00000001 – program 'RESTART'), and the National Centre for HPC, Big Data and Quantum Computing (CN00000013 – CUP E13C22000990001).

Data availability statement

All data that support the findings of this study are included within the article (and any supplementary files).

Appendix A. Cavity eigenfrequencies

By equating the denominator of $D(\omega)$ with the product $(\omega-\omega_+)(\omega+\omega_+^*)(\omega-\omega_-)(\omega+\omega_-^*)$ and requiring that the poles have the form

$$\omega_\pm = \omega_c \pm \zeta + \Sigma - \mathrm{i}\Gamma/2, \tag{A1}$$

in [18] we obtained

$$\zeta^2 = \frac{\omega_c^2}{2} + \frac{\tau^2}{4} - \frac{3}{32}\gamma_D^2 - \frac{1}{8}\sqrt{16\omega_c^4 - \gamma_D^2\left(2\omega_c^2 + \tau^2 + \frac{5}{16}\gamma_D^2\right)}, \tag{A2}$$

$$\Sigma = -\omega_c + \frac{1}{2}\left[2\omega_c^2 + \tau^2 - \frac{3}{8}\gamma_D^2 + 2\sqrt{\omega_c^4 - \frac{1}{16}\left[(2\omega_c^2+\tau^2)\gamma_D^2 + 5\gamma_D^4\right]}\right]^{1/2},$$

$$\Gamma = \gamma_D/2, \tag{A3}$$

where $\tau \equiv \xi\Omega_{pl}$ is the light-matter (EC-SPP) coupling strength. The frequencies separation,

$$(\omega_+ - \omega_-)_{\omega_{pl}=\omega_c} = 2\zeta, \tag{A4}$$

is set entirely by the parameter ζ (the common shift Σ cancels), which depends on the losses. In the lossless limit, we recover $\zeta = \tau/2$.

Appendix B. Component rate equations

For numerical integration we use the time-local GKSL master equation equations (23) and (24) in the truncated polariton Fock space $n_\pm \leqslant 1$. Although equations (26)–(28) provide a compact vectorized form, for numerical simulations it is necessary to write the corresponding system of coupled first-order ODEs for the density-matrix elements explicitly, in a form tailored to the bright and dark projectors $\hat{P}_\mathrm{b}, \hat{P}_\mathrm{d}$.

Basis and operators. We work in the rotated basis $\{|\mathrm{g}\rangle, |\mathrm{b}\rangle, |\mathrm{d}\rangle, |\mathrm{e}\rangle\}$, where $|\mathrm{b}\rangle = (|+\rangle + |-\rangle)/\sqrt{2}$ and $|\mathrm{d}\rangle = (|+\rangle - |-\rangle)/\sqrt{2}$. In this basis, $\langle \hat{P}_\mathrm{b}(t)\rangle = \rho_\mathrm{bb}(t)$ and $\langle \hat{P}_\mathrm{d}(t)\rangle = \rho_\mathrm{dd}(t)$ with $\hat{P}_\mathrm{b} = |\mathrm{b}\rangle\langle\mathrm{b}|$ and $\hat{P}_\mathrm{d} = |\mathrm{d}\rangle\langle\mathrm{d}|$.

The truncated lowering operators are

$$\begin{aligned} \hat{B}_\mathrm{b} &= |\mathrm{g}\rangle\langle\mathrm{b}| + |\mathrm{b}\rangle\langle\mathrm{e}|, \\ \hat{B}_\mathrm{d} &= |\mathrm{g}\rangle\langle\mathrm{d}| - |\mathrm{d}\rangle\langle\mathrm{e}|, \end{aligned} \tag{B1}$$

so that $\hat{B}_\mathrm{b}^\dagger \hat{B}_\mathrm{b} = |\mathrm{b}\rangle\langle\mathrm{b}| + |\mathrm{e}\rangle\langle\mathrm{e}|$ and $\hat{B}_\mathrm{d}^\dagger \hat{B}_\mathrm{d} = |\mathrm{d}\rangle\langle\mathrm{d}| + |\mathrm{e}\rangle\langle\mathrm{e}|$. In the symmetric rotating frame of the central drive frequency, the system Hamiltonian $\hat{H}_\mathrm{s}$ takes the form

$$\hat{H}_\mathrm{s} = \frac{\Delta}{2}\left(|\mathrm{b}\rangle\langle\mathrm{d}| + |\mathrm{d}\rangle\langle\mathrm{b}|\right), \tag{B2}$$

where $\Delta = \omega_+ - \omega_-$ as in the main text (including, if desired, the corresponding Lamb shifts we always omit). The (piecewise) coherent drive alternates between the bright $\hat{H}_\mathrm{drive}^{(\mathrm{b})}$ and dark $\hat{H}_\mathrm{drive}^{(\mathrm{d})}$ drives,

$$\begin{aligned} \hat{H}_\mathrm{drive}^{(\mathrm{b})} &= \sqrt{2} f(t)\left(\hat{B}_\mathrm{b} + \hat{B}_\mathrm{b}^\dagger\right), \\ \hat{H}_\mathrm{drive}^{(\mathrm{d})} &= \sqrt{2} f(t)\left(\hat{B}_\mathrm{d} + \hat{B}_\mathrm{d}^\dagger\right), \end{aligned} \tag{B3}$$

with real $f(t)$ (piecewise constant in the numerical examples).

Leakage dissipator in the symmetric case. To keep the comparison transparent, we specialize equation (35) to the symmetric case $J(\omega_+) = J(\omega_-) \equiv \Gamma$. In the $\{\hat{B}_+, \hat{B}_-\}$ basis, the corresponding 2×2 Kossakowski matrix becomes

$$\widetilde{W} = \begin{pmatrix} \Gamma & g \\ g & \Gamma \end{pmatrix}, \qquad g = \kappa_\mathrm{c}\Gamma. \tag{B4}$$

The eigenvectors are the symmetric/antisymmetric combinations, yielding the jump operators

$$\hat{Q}_\mathrm{b} = \frac{\hat{B}_+ + \hat{B}_-}{\sqrt{2}} \equiv \hat{B}_\mathrm{b}, \qquad \hat{Q}_\mathrm{d} = \frac{\hat{B}_+ - \hat{B}_-}{\sqrt{2}} \equiv \hat{B}_\mathrm{d}, \tag{B5}$$

with corresponding rates

$$\Gamma_\mathrm{b} = \Gamma + g = \Gamma(1+\kappa_\mathrm{c}), \qquad \Gamma_\mathrm{d} = \Gamma - g = \Gamma(1-\kappa_\mathrm{c}). \tag{B6}$$

Substituting these into equation (20*b*) gives

$$\mathcal{L}_\mathrm{leak}^{(\mathrm{ns})}\hat{\rho} = \Gamma_\mathrm{b}\mathcal{D}\left[\hat{B}_\mathrm{b}\right]\hat{\rho} + \Gamma_\mathrm{d}\mathcal{D}\left[\hat{B}_\mathrm{d}\right]\hat{\rho}. \tag{B7}$$

In the secular approximation the cross term is dropped ($g = 0$), so that $\Gamma_\mathrm{b} = \Gamma_\mathrm{d} \equiv \Gamma$. Additional channels (UP↔LP scattering and pure dephasing) can be included by adding the corresponding $\gamma_k\mathcal{D}[\hat{L}_k]$ and $\gamma_\phi\mathcal{D}[\hat{N}_\pm]$ terms as in equation (24), although here we focus on the leakage-only case. Using equation (25), the vectorized ODE equation (26) is equivalent to

$$\dot{\rho}_{mn} = -\mathrm{i}\sum_k\left(H_{mk}\rho_{kn} - \rho_{mk}H_{kn}\right) + \sum_j \Gamma_j\left[\left(J_j\rho J_j^\dagger\right)_{mn} - \tfrac{1}{2}\left(J_j^\dagger J_j\rho + \rho J_j^\dagger J_j\right)_{mn}\right], \tag{B8}$$

where $m,n,k \in \{\mathrm{g},\mathrm{b},\mathrm{d},\mathrm{e}\}$, $\hat{H} = \hat{H}_\mathrm{s} + \hat{H}_\mathrm{drive}$, and $\{J_j\} = \{\hat{B}_\mathrm{b}, \hat{B}_\mathrm{d}\}$ with rates $\{\Gamma_j\} = \{\Gamma_\mathrm{b}, \Gamma_\mathrm{d}\}$. The resulting closed subsystem of equations for the independent matrix elements (the remaining elements follow from Hermiticity, $\rho_{mn} = \rho_{nm}^*$, and $\mathrm{Tr}\,\rho = 1$) depends on the type of drive. For the bright drive it is:

$$\dot{\rho}_\mathrm{gg} = \Gamma_\mathrm{b}\rho_\mathrm{bb} + \Gamma_\mathrm{d}\rho_\mathrm{dd} + \sqrt{2}\,\mathrm{i}f\left(\rho_\mathrm{gb} - \rho_\mathrm{bg}\right), \tag{B9}$$

$$\dot{\rho}_{\mathrm{bb}} = -\Gamma_{\mathrm{b}}\left(\rho_{\mathrm{bb}} - \rho_{\mathrm{ee}}\right) + \mathrm{i}\frac{\Delta}{2}\left(\rho_{\mathrm{bd}} - \rho_{\mathrm{db}}\right) + \sqrt{2}\mathrm{i}f\left(\rho_{\mathrm{bg}} - \rho_{\mathrm{gb}} + \rho_{\mathrm{be}} - \rho_{\mathrm{eb}}\right), \tag{B10}$$

$$\dot{\rho}_{\mathrm{dd}} = -\Gamma_{\mathrm{d}}\left(\rho_{\mathrm{dd}} - \rho_{\mathrm{ee}}\right) + \mathrm{i}\frac{\Delta}{2}\left(\rho_{\mathrm{db}} - \rho_{\mathrm{bd}}\right), \tag{B11}$$

$$\dot{\rho}_{\mathrm{ee}} = -\left(\Gamma_{\mathrm{b}} + \Gamma_{\mathrm{d}}\right)\rho_{\mathrm{ee}} + \sqrt{2}\mathrm{i}f\left(\rho_{\mathrm{eb}} - \rho_{\mathrm{be}}\right), \tag{B12}$$

$$\dot{\rho}_{\mathrm{gb}} = -\frac{\Gamma_{\mathrm{b}}}{2}\rho_{\mathrm{gb}} + \Gamma_{\mathrm{b}}\rho_{\mathrm{be}} + \mathrm{i}\frac{\Delta}{2}\rho_{\mathrm{gd}} + \mathrm{i}\sqrt{2}f\left(\rho_{\mathrm{gg}} + \rho_{\mathrm{ge}} - \rho_{\mathrm{bb}}\right), \tag{B13}$$

$$\dot{\rho}_{\mathrm{gd}} = -\frac{\Gamma_{\mathrm{d}}}{2}\rho_{\mathrm{gd}} - \Gamma_{\mathrm{d}}\rho_{\mathrm{de}} + \mathrm{i}\frac{\Delta}{2}\rho_{\mathrm{gb}} - \mathrm{i}\sqrt{2}f\rho_{\mathrm{bd}}, \tag{B14}$$

$$\dot{\rho}_{\mathrm{ge}} = -\frac{\Gamma_{\mathrm{b}} + \Gamma_{\mathrm{d}}}{2}\rho_{\mathrm{ge}} + \mathrm{i}\sqrt{2}f\left(\rho_{\mathrm{gb}} - \rho_{\mathrm{be}}\right), \tag{B15}$$

$$\dot{\rho}_{\mathrm{bd}} = -\frac{\Gamma_{\mathrm{b}} + \Gamma_{\mathrm{d}}}{2}\rho_{\mathrm{bd}} + \mathrm{i}\frac{\Delta}{2}\left(\rho_{\mathrm{bb}} - \rho_{\mathrm{dd}}\right) - \mathrm{i}\sqrt{2}f\left(\rho_{\mathrm{gd}} + \rho_{\mathrm{ed}}\right), \tag{B16}$$

$$\dot{\rho}_{\mathrm{be}} = -\left(\Gamma_{\mathrm{b}} + \frac{\Gamma_{\mathrm{d}}}{2}\right)\rho_{\mathrm{be}} - \mathrm{i}\frac{\Delta}{2}\rho_{\mathrm{de}} - \mathrm{i}\sqrt{2}f\left(\rho_{\mathrm{ge}} - \rho_{\mathrm{bb}} + \rho_{\mathrm{ee}}\right), \tag{B17}$$

$$\dot{\rho}_{\mathrm{de}} = -\left(\Gamma_{\mathrm{d}} + \frac{\Gamma_{\mathrm{b}}}{2}\right)\rho_{\mathrm{de}} - \mathrm{i}\frac{\Delta}{2}\rho_{\mathrm{be}} + \mathrm{i}\sqrt{2}f\rho_{\mathrm{db}}, \tag{B18}$$

and similarly for the dark drive. The solutions shown in figures 2–4 are obtained by integrating the above ODEs (with the appropriate choice of $\Gamma_{\mathrm{b}}, \Gamma_{\mathrm{d}}$ for the non-secular description, or $\Gamma_{\mathrm{b}} = \Gamma_{\mathrm{d}}$ for the secular approximation) and then evaluating $\rho_{\mathrm{bb}}(t)$ and $\rho_{\mathrm{dd}}(t)$.

Appendix C. Steady-state solution in the truncated polariton space

We work in the truncated polariton Fock space $n_{\pm} \leqslant 1$ (dimension $d = 4$), spanned by

$$\{|\mathrm{g}\rangle, |-\rangle, |+\rangle, |\mathrm{e}\rangle\} \equiv \{|0,0\rangle, |0,1\rangle, |1,0\rangle, |1,1\rangle\}, \tag{C1}$$

with $|\mathrm{g}\rangle$ the vacuum and $|\mathrm{e}\rangle$ the double-excitation state. The bright and dark states $|\mathrm{b}\rangle, |\mathrm{d}\rangle$ and the projectors $\hat{P}_{\mathrm{b}}, \hat{P}_{\mathrm{d}}$ are defined in the main text according to equations (29)–(31). In the $\{|+\rangle, |-\rangle\}$ basis,

$$\begin{aligned}\langle\hat{P}_{\mathrm{b}}\rangle &= \tfrac{1}{2}\left(\rho_{++} + \rho_{--} + \rho_{+-} + \rho_{-+}\right),\\ \langle\hat{P}_{\mathrm{d}}\rangle &= \tfrac{1}{2}\left(\rho_{++} + \rho_{--} - \rho_{+-} - \rho_{-+}\right),\end{aligned} \tag{C2}$$

where $\rho_{mn} \equiv \langle m|\hat{\rho}|n\rangle$ $(m, n \in \{\mathrm{g}, -, +, \mathrm{e}\})$.

In the $\{|+\rangle, |-\rangle\}$ basis, the piecewise coherent drive used throughout this work can be written as

$$\begin{aligned}\hat{H}^{(\eta)}_{\mathrm{drive}} &= f\left(\hat{B}_{+} + \eta\hat{B}_{-} + \hat{B}^{\dagger}_{+} + \eta\hat{B}^{\dagger}_{-}\right),\\ \eta &= \begin{cases} +1 & \text{(bright drive)}\\ -1 & \text{(dark drive)}.\end{cases}\end{aligned} \tag{C3}$$

Thus the branch-resolved drive amplitudes f_{μ} are $f_{+} = f$ and $f_{-} = \eta f$. For clarity, for the bright drive $(\eta = +1)$ one has $f_{+} = f_{-} = f$, whereas for the dark drive $(\eta = -1)$ $f_{+} = f$ and $f_{-} = -f$.

C.1. Secular approximation

In the secular approximation, the two polariton branches evolve independently and the steady state (ss) factorizes, $\rho^{(\mathrm{sec})}_{\mathrm{ss}} = \rho^{(+)}_{\mathrm{ss}} \otimes \rho^{(-)}_{\mathrm{ss}}$. For each branch $\mu \in \{+, -\}$, we truncate to $\mathcal{H}^{(2)}_{\mu} = \mathrm{span}\{|\mathrm{g}\rangle, |\mu\rangle\}$ and define $\hat{\sigma}^{(\mu)} \equiv |\mathrm{g}\rangle\langle\mu|$ and $\hat{\sigma}^{(\mu)\dagger} \equiv |\mu\rangle\langle\mathrm{g}|$. In the rotating frame of the drive at $\omega_{\mathrm{c}} \equiv \omega_{\mathrm{pl}}$, the reduced density matrix $\rho^{(\mu)}$ obeys

$$\dot{\rho}^{(\mu)} = -\mathrm{i}\left[H^{(\mu)}, \rho^{(\mu)}\right] + \Gamma_{\mu}\mathcal{D}\left[\hat{\sigma}^{(\mu)}\right]\rho^{(\mu)}, \tag{C4}$$

$$H^{(\mu)} = \delta_{\mu}|\mu\rangle\langle\mu| + f_{\mu}\left(\hat{\sigma}^{(\mu)\dagger} + \hat{\sigma}^{(\mu)}\right), \tag{C5}$$

where $\delta_{\mu} \equiv \omega_{\mu} - \omega_{\mathrm{c}}$ and, in our symmetric setup, $\delta_{\pm} = \pm\Delta/2$.

Let $p_{\mu} \equiv \rho^{(\mu)}_{\mu\mu}$ and $s_{\mu} \equiv \rho^{(\mu)}_{\mu\mathrm{g}}$. From equation (C4) one obtains the optical Bloch equations

$$\dot{p}_{\mu} = -\Gamma_{\mu}p_{\mu} + \mathrm{i}f_{\mu}\left(s^{*}_{\mu} - s_{\mu}\right), \tag{C6}$$

$$\dot{s}_\mu = -\left(\frac{\Gamma_\mu}{2} + \mathrm{i}\delta_\mu\right) s_\mu + \mathrm{i} f_\mu \left(2p_\mu - 1\right). \tag{C7}$$

Setting $\dot{s}_\mu = 0$ gives

$$s_\mu = \mathrm{i} f_\mu \frac{2p_\mu - 1}{\frac{\Gamma_\mu}{2} + \mathrm{i}\delta_\mu}, \tag{C8}$$

which implies

$$\mathrm{i} f_\mu \left(s_\mu^* - s_\mu\right) = \Gamma_\mu \frac{4f_\mu^2}{\Gamma_\mu^2 + 4\delta_\mu^2} \left(1 - 2p_\mu\right). \tag{C9}$$

Inserting equation (C9) into $\dot{p}_\mu = 0$ yields

$$p_\mu = \frac{4f_\mu^2}{\Gamma_\mu^2 + 4\delta_\mu^2 + 8f_\mu^2}, \tag{C10}$$

and substituting back into equation (C8) gives the stationary coherence

$$s_\mu = -\frac{2f_\mu \left(2\delta_\mu + \mathrm{i}\Gamma_\mu\right)}{\Gamma_\mu^2 + 4\delta_\mu^2 + 8f_\mu^2}. \tag{C11}$$

The factorized structure gives the steady-state matrix elements in the global basis:

$$\begin{aligned} &\rho_{++} = p_+ \left(1 - p_-\right), \qquad \rho_{--} = p_- \left(1 - p_+\right), \\ &\rho_{+-} = s_+ s_-^*, \end{aligned} \tag{C12}$$

so that the coherences ρ_{+-} and $\rho_{-+} = \rho_{+-}^*$ are generally nonzero even though $\rho_{\mathrm{ss}}^{(\mathrm{sec})}$ factorizes.

For the symmetric case, $\Gamma_\mu \equiv \Gamma$ according to equation (11), with $\delta_\pm = \pm\Delta/2$ and $f_+ = f$, $f_- = \eta f$, it is convenient to define

$$D = \Gamma^2 + \Delta^2 + 8f^2. \tag{C13}$$

A short algebra using equations (C2) and (C10)–(C12) yields

$$\begin{aligned} \langle \hat{P}_\mathrm{b} \rangle_{\mathrm{ss}}^{(\mathrm{sec})} \big|_{\eta=1} &= \frac{4f^2}{D^2} \left(2\Gamma^2 + 4f^2\right), \\ \langle \hat{P}_\mathrm{d} \rangle_{\mathrm{ss}}^{(\mathrm{sec})} \big|_{\eta=1} &= \frac{4f^2}{D^2} \left(2\Delta^2 + 4f^2\right), \end{aligned} \tag{C14}$$

for the bright drive, while for the dark drive the two expressions are exchanged,

$$\begin{aligned} \langle \hat{P}_\mathrm{b} \rangle_{\mathrm{ss}}^{(\mathrm{sec})} \big|_{\eta=-1} &= \langle \hat{P}_\mathrm{d} \rangle_{\mathrm{ss}}^{(\mathrm{sec})} \big|_{\eta=1} \\ \langle \hat{P}_\mathrm{d} \rangle_{\mathrm{ss}}^{(\mathrm{sec})} \big|_{\eta=-1} &= \langle \hat{P}_\mathrm{b} \rangle_{\mathrm{ss}}^{(\mathrm{sec})} \big|_{\eta=1}. \end{aligned} \tag{C15}$$

C.2. Non-secular leakage

The diagonal form equation (B7), expressed in terms of the bright and dark jump operators $\hat{B}_{\mathrm{b},d} = (\hat{B}_+ \pm \hat{B}_-)/\sqrt{2}$, and the closed-form steady-state expressions derived below, assume an unresolved-transition (common-bath) regime $|\Delta| \lesssim \gamma_\mathrm{D}/2$, so that the suppression factor κ_c in equation (35) remains close to unity. In this limit, the bath does not resolve the two Bohr frequencies $\omega_\pm = \omega_\mathrm{c} \pm \Delta/2$, so $J(\omega_+) \simeq J(\omega_-)$ and the off-diagonal Kossakowski element g remains appreciable; the dissipator is then well diagonalized by the bright (symmetric) and dark (antisymmetric) superpositions. For $|\Delta| \gg \gamma_\mathrm{D}/2$ (so that $\kappa_\mathrm{c} \to 0$), the cross correlations are suppressed ($g \to 0$) and the natural jump operators approach $\hat{B}_\pm$ instead, so the bright and dark ladder solution we report below is no longer quantitative.

Moreover, in the analytical solutions presented here, we neglect the coherent $b \leftrightarrow d$ mixing induced by $\hat{H}_s = \frac{\Delta}{2}(\hat{N}_+ - \hat{N}_-)$ when expressed in the $\{|\mathrm{b}\rangle, |\mathrm{d}\rangle\}$ basis, an effect that becomes relevant as Δ increases. Instead, the complete numerical solutions presented in the main text describe the correct physics. This restriction applies only to the closed-form ladder steady states reported below. The component rate equations (and the numerical GKSL integration) remain valid for arbitrary Δ, and for $\Delta \gg \gamma_\mathrm{D}/2$, the non-secular generator continuously approaches the secular one as $g \to 0$.

Therefore, limiting the validity of the following discussion to the case $\Delta \lesssim \gamma_{\mathbf{D}}/2$, we use equations (29) and (30) to write the Hamiltonian for the bright and dark drives as

$$\hat{H}_{\text{drive}}^{(\eta=1)} = \sqrt{2}f\left(\hat{B}_{\text{b}} + \hat{B}_{\text{b}}^{\dagger}\right), \qquad \text{bright drive}$$
$$\hat{H}_{\text{drive}}^{(\eta=-1)} = \sqrt{2}f\left(\hat{B}_{\text{d}} + \hat{B}_{\text{d}}^{\dagger}\right), \qquad \text{dark drive.} \tag{C16}$$

For a given drive choice η, the master equation is

$$\dot{\hat{\rho}} = -\text{i}\left[\hat{H}_{\text{drive}}^{(\eta)}, \hat{\rho}\right] + \mathcal{L}_{\text{leak}}^{(\text{ns})}\hat{\rho}. \tag{C17}$$

In this subsection it is more useful to work in the basis $\{|\text{g}\rangle, |\text{b}\rangle, |\text{d}\rangle, |\text{e}\rangle$ and use $\rho_{mn} \equiv \langle m|\hat{\rho}|n\rangle$ with $m, n \in$ g, b, d, e.

Bright drive. For $\eta = 1$, the Hamiltonian couples the resonant ladder $|\text{g}\rangle \leftrightarrow |\text{b}\rangle \leftrightarrow |\text{e}\rangle$, while $|\text{d}\rangle$ is populated only via the decay $|\text{e}\rangle \to |\text{d}\rangle$ generated by $\hat{B}_{\text{d}}$. The equations of motion for the populations and the coherences needed to close the system are

$$\dot{\rho}_{\text{dd}} = \Gamma_{\text{d}}\left(\rho_{\text{ee}} - \rho_{\text{dd}}\right), \tag{C18}$$
$$\dot{\rho}_{\text{ee}} = -\left(\Gamma_{\text{b}} + \Gamma_{\text{d}}\right)\rho_{\text{ee}} - \text{i}\sqrt{2}f\left(\rho_{\text{be}} - \rho_{\text{eb}}\right), \tag{C19}$$
$$\dot{\rho}_{\text{bb}} = -\Gamma_{\text{b}}\left(\rho_{\text{bb}} - \rho_{\text{ee}}\right) - \text{i}\sqrt{2}f\left(\rho_{\text{gb}} - \rho_{\text{bg}} - \rho_{\text{be}} + \rho_{\text{eb}}\right), \tag{C20}$$
$$\dot{\rho}_{\text{gb}} = -\frac{\Gamma_{\text{b}}}{2}\rho_{\text{gb}} + \Gamma_{\text{b}}\rho_{\text{be}} + \text{i}\sqrt{2}f\left(\rho_{\text{gg}} + \rho_{\text{ge}} - \rho_{\text{bb}}\right), \tag{C21}$$
$$\dot{\rho}_{\text{be}} = -\left(\Gamma_{\text{b}} + \frac{\Gamma_{\text{d}}}{2}\right)\rho_{\text{be}} - \text{i}\sqrt{2}f\left(\rho_{\text{ge}} - \rho_{\text{bb}} + \rho_{\text{ee}}\right), \tag{C22}$$
$$\dot{\rho}_{\text{ge}} = -\frac{\Gamma_{\text{b}} + \Gamma_{\text{d}}}{2}\rho_{\text{ge}} + \text{i}\sqrt{2}f\left(\rho_{\text{gb}} - \rho_{\text{be}}\right), \tag{C23}$$

with $\rho_{\text{gg}} = 1 - \rho_{\text{bb}} - \rho_{\text{dd}} - \rho_{\text{ee}}$. At steady state, equation (C18) gives $\rho_{\text{dd}} = \rho_{\text{ee}}$; eliminating the coherences from equations(C19)–(C23) yields two algebraic equations for ρ_{bb} and ρ_{ee}, whose solution can be written compactly as

$$\rho_{\text{bb}}^{(\text{ns})} = \frac{32f^2\left[\Gamma^2 + 2f^2\right]}{\mathcal{N}_{\text{b}}}, \qquad \rho_{\text{dd},ee}^{(\text{ns})} = \frac{64f^4}{\mathcal{N}_{\text{b}}} \tag{C24}$$

where $\mathcal{N}_{\text{b}} = 4\Gamma^2\left(\Gamma_{\text{b}}^2 + 16f^2\right) + (4f)^4$, having also exploited $\Gamma_{\text{b}} + \Gamma_{\text{d}} = 2\Gamma$. Since $\hat{P}_{\text{b}} = |\text{b}\rangle\langle\text{b}|$ and $\hat{P}_{\text{d}} = |\text{d}\rangle\langle\text{d}|$ in the single-excitation manifold, one has $\langle\hat{P}_{\text{b}}\rangle_{\text{ss}}^{(\text{ns})} = \rho_{\text{bb}}^{(\text{ns})}$ and $\langle\hat{P}_{\text{d}}\rangle_{\text{ss}}^{(\text{ns})} = \rho_{\text{dd}}^{(\text{ns})}$.

Dark drive. For $\eta = -1$, the same derivation applies upon exchanging b $\leftrightarrow$ d, i.e.

$$\rho_{\text{bb},ee}^{(\text{ns})} = \frac{64f^4}{\mathcal{N}_{\text{b}}}, \qquad \rho_{\text{dd}}^{(\text{ns})} = \frac{32f^2\left[\Gamma^2 + 2f^2\right]}{\mathcal{N}_{\text{d}}}, \tag{C25}$$

where $\mathcal{N}_{\text{d}} = 4\Gamma^2\left(\Gamma_{\text{d}}^2 + 16f^2\right) + (4f)^4$, so that $\langle\hat{P}_{\text{b}}\rangle_{\text{ss}}^{(\text{ns})} = \rho_{\text{bb}}^{(\text{ns})}$ and $\langle\hat{P}_{\text{d}}\rangle_{\text{ss}}^{(\text{ns})} = \rho_{\text{dd}}^{(\text{ns})}$.

ORCID iD

Marco Vallone 0000-0003-3392-1810

References

[1] Raether H 1988 Springer Tracts in Modern Physics *Surface Plasmons on Smooth and Rough Surfaces and on Gratings* vol 111 (Springer)
[2] Biagioni P, Huang J-S and Hecht B 2012 Nanoantennas for visible and infrared radiation *Rep. Prog. Phys.* **75** 024402
[3] Palaferri D, Todorov Y, Chen Y N, Madeo J, Vasanelli A, Li L H, Davies A G, Linfield E H and Sirtori C 2015 Patch antenna terahertz photodetectors *Appl. Phys. Lett.* **106** 161102
[4] Iqbal T, Khalil S, Ijaz M, Riaz K N, Khan M I, Shakil M, Nabi A G, Javaid M, Abrar M and Afsheen S 2019 Optimization of 1D plasmonic grating of nanostructured devices for the investigation of plasmonic bandgap *Plasmonics* **14** 775
[5] Kockum A F, Miranowicz A, Liberato S D, Savasta S and Nori F 2019 Ultrastrong coupling between light and matter *Nat. Rev. Phys.* **1** 19

[6] Baranov D G, Munkhbat B, Zhukova E, Bisht A, Canales A, Rousseaux B, Johansson G, Antosiewicz T J and Shegai T 2020 Ultrastrong coupling between nanoparticle plasmons and cavity photons at ambient conditions *Nat. Commun.* **11** 2715

[7] Yoo D, de León-Pérez F, Lee I-H, Mohr D A, Raschke M B, Caldwell J D, Martín-Moreno L and Oh S H 2021 Ultrastrong plasmon–phonon coupling via epsilon-near-zero nanocavities *Nat. Photon.* **15** 125

[8] Wang Z, Li L, Wei S, Shi X, Xiao J, Guo Z, Wang W, Wang Y and Wang W 2023 Manipulating light-matter interaction into strong coupling regime for photon entanglement in plasmonic lattices *J. Appl. Phys.* **133** 063101

[9] Hopfield J J 1958 Theory of the contribution of excitons to the complex dielectric constant of crystals *Phys. Rev.* **112** 1555

[10] Ciuti C, Bastard G and Carusotto I 2005 Quantum vacuum properties of the intersubband cavity polariton field *Phys. Rev. B* **72** 115303

[11] Vasanelli A, Todorov Y and Sirtori C 2016 Ultra-strong light-matter coupling and superradiance using dense electron gases *C. R. Phys.* **17** 861

[12] Liu A 1997 Rabi splitting of the optical intersubband absorption line of multiple quantum wells inside a Fabry-Pérot microcavity *Phys. Rev. B* **55** 7101

[13] Todorov Y, Andrews A M, Colombelli R, Liberato S D, Ciuti C, Klang P, Strasser G and Sirtori C 2010 Optical properties of metal-dielectric-metal microcavities in the THz frequency range *Opt. Express* **18** 13886

[14] Feuillet-Palma C, Todorov Y, Vasanelli A and Sirtori C 2013 Strong near field enhancement in THz nano-antenna arrays *Sci. Rep.* **3** 1361

[15] Manceau J-M, Biasiol G, Tran N L, Carusotto I and Colombelli R 2017 Immunity of intersubband polaritons to inhomogeneous broadening *Phys. Rev. B* **96** 235301

[16] Vigneron P-B, Pirotta S, Carusotto I, Tran N-L, Biasiol G, Manceau J-M, Bousseksou A and Colombelli R 2019 Quantum well infrared photo-detectors operating in the strong light-matter coupling regime *Appl. Phys. Lett.* **114** 131104

[17] Pisani F, Gacemi D, Vasanelli A, Li L, Davies A G, Linfield E, Sirtori C and Todorov Y 2023 Electronic transport driven by collective light-matter coupled states in a quantum device *Nat. Commun.* **14** 3914

[18] Vallone M 2026 Quantum open system description of a hybrid plasmonic cavity *Phys. Rev. A* **113** 033723

[19] Lindblad G 1976 On the generators of quantum dynamical semigroups *Commun. Math. Phys.* **48** 119

[20] Gorini V, Kossakowski A and Sudarshan E C G 1976 Completely positive dynamical semigroups of n-level systems *J. Math. Phys.* **17** 821

[21] Breuer H P and Petruccione F 2007 *The Theory of Open Quantum Systems* (Oxford University Press)

[22] Vallone M 2025 Renormalized photon propagator in quantum electrodynamics of plasmonic cavities *New J. Phys* **27** 064102

[23] Beaudoin F, Gambetta J M and Blais A 2011 Dissipation and ultrastrong coupling in circuit QED *Phys. Rev. A* **84** 043832

[24] Hu D, Huang S Y, Liao J Q, Tian L and Goan H S 2015 Quantum coherence in ultrastrong optomechanics *Phys. Rev. A* **91** 013812

[25] De Bernardis D, Pilar P, Jaako T, Liberato S D and Rabl P 2018 Breakdown of gauge invariance in ultrastrong-coupling cavity QED *Phys. Rev. A* **98** 053819

[26] de la Pradilla D F, Moreno E and Feist J 2024 Recovering an accurate Lindblad equation from the Bloch-Redfield equation for general open quantum systems *Phys. Rev. A* **109** 062225

[27] Lednev M, García-Vidal F J and Feist J 2024 Lindblad master equation capable of describing hybrid quantum systems in the ultrastrong coupling regime *Phys. Rev. Lett.* **132** 106902

[28] Chong Y D and Soljačić M 2008 Dark-state polaritons in single- and double-Λ media *Phys. Rev. A* **77** 013823

[29] Kim B, Chen K-T, Chen K-Y, Chiu Y-S, Hsu C-Y, Chen Y-H and Yu I-A 2023 Experimental demonstration of stationary dark-state polaritons dressed by dipole-dipole interaction *Phys. Rev. Lett.* **131** 133001

[30] Bouteyre P, Hu X, Randerson S A, Zotev P G, Wang Y and Tartakovskii A I 2025 Simultaneous observation of bright and dark polariton states in subwavelength gratings made from quasi-bulk WS2 *Opt. Express* **33** 21173

[31] Liu J and Li Z-Y 2014 Interaction of a two-level atom with single-mode optical field beyond the rotating wave approximation *Opt. Express* **22** 28671

[32] Liu Z, Li J, Liu Z, Li W, Li J, Gu C and Li Z-Y 2017 Fano resonance Rabi splitting of surface plasmons *Sci. Rep.* **7** 8010

[33] Todorov Y and Sirtori C 2012 Intersubband polaritons in the electrical dipole gauge *Phys. Rev. B* **85** 045304

[34] Vukics A, Konya G and Domokos P 2021 The gauge-invariant Lagrangian, the Power-Zienau-Woolley picture and the choices of field momenta in nonrelativistic quantum electrodynamics *Sci. Rep.* **11** 16337

[35] Hartmann R and Strunz W T 2020 Accuracy assessment of perturbative master equations: embracing nonpositivity *Phys. Rev. A* **101** 012103

[36] Eastham P R, Kirton P, Cammack H M, Lovett B W and Keeling J 2016 Bath-induced coherence and the secular approximation *Phys. Rev. A* **94** 012110

[37] Callen H B and Welton T A 1951 Irreversibility and generalized noise *Phys. Rev.* **83** 34

[38] Kubo R 1966 The fluctuation-dissipation theorem *Rep. Prog. Phys.* **29** 255

[39] Weiss U 2012 *Quantum Dissipative Systems* 4th edn (World Scientific)

[40] More specifically, we define $\int_0^\infty d\tau\, e^{i\omega\tau} C(\tau) = \frac{1}{2}\gamma(\omega) + i\lambda(\omega)$. For a bosonic bath with spectral density $J(\omega)$ in thermal equilibrium, $C(t) = \int_0^\infty d\omega' J(\omega') \left\{ [n(\omega')+1] e^{-i\omega' t} + n(\omega') e^{i\omega' t} \right\}$., where $n(\omega)$ is the Bose distribution. This yields $\gamma(\omega) \propto J(\omega)[n(\omega)+1]$ for $\omega > 0$ and $\gamma(\omega) \propto J(|\omega|)n(|\omega|)$ for $\omega < 0$, while $\lambda(\omega)$ is a principal-value integral over $J(\omega)$ (its Hilbert transform). At zero temperature, equations (14) and (15) follow.

[41] Inserting $\hat{H}_{\rm int}(t) = \hat{X}(t) \otimes \hat{\mathcal{B}}(t)$ into the Born–Markov master equation and tracing over the environment, characterized by a density operator $\hat{\rho}_{\rm env}$, yields bath correlation functions $C(\tau) = {\rm Tr}_{\rm env}[\hat{\mathcal{B}}(\tau)\hat{\mathcal{B}}(0)\hat{\rho}_{\rm env}]$ multiplied by products of system operators $\hat{X}(t)$ and $\hat{X}(t-\tau)$ [21] Thus, the reservoir operator $\hat{\mathcal{B}}$ disappears from the reduced dynamics, surviving only through the scalar functions $\gamma(\omega)$ and $\lambda(\omega)$ obtained from $C(\tau)$ (or equivalently from the spectral density $J(\omega)$ associated with the Drude–Lorentz susceptibility), while the Bloch–Redfield tensors $\Gamma_{ij}(\omega)$ and $\Lambda_{ij}(\omega)$ arise from combining these scalar kernels with the system coefficients $A_i^* A_j$ that weight the transition operators $\hat{\sigma}_j$.

[42] Johansson J, Nation P and Nori F 2012 QuTiP: an open-source python framework for the dynamics of open quantum systems *Comp. Phys. Commun.* **183** 1760

[43] Johansson J, Nation P and Nori F 2013 QuTiP 2: a python framework for the dynamics of open quantum systems *Comp. Phys. Commun.* **184** 1234

[44] Gu J and Zhang F 2025 Generic method for integrating Lindblad master equations *Phys. Rev. E* **112** 044106

[45] Am-Shallem M, Levy A, Schaefer I and Kosloff R 2015 Three approaches for representing Lindblad dynamics by a matrix-vector notation (arXiv:1510.08634)

[46] For a lorentzian spectrum of FWHM $\gamma_{\rm D}$ the bath correlation function decays as $C(\tau) \propto {\rm e}^{-(\gamma_{\rm D}/2)\tau}$ (up to a carrier oscillation at $\omega_{\rm pl}$), and the oscillatory cross term carrying the beat phase ${\rm e}^{{\rm i}Delta\tau}$ is reduced by the normalized overlap

$$\kappa_{\rm c} = \frac{\int_0^\infty {\rm d}\tau\, {\rm e}^{-(\gamma_{\rm D}/2)\tau} \cos(\Delta\tau)}{\int_0^\infty {\rm d}\tau\, {\rm e}^{-(\gamma_{\rm D}/2)\tau}} = \frac{(\gamma_{\rm D}/2)^2}{(\gamma_{\rm D}/2)^2+\Delta^2}.$$

[47] For a single-peaked spectral density, e.g., a Lorentzian $J(\omega) = J_0\omega/[(\omega-\omega_0)^2+\gamma_{\rm D}^2]$, taking two transition frequencies $\omega_i = \omega_0$ and $\omega_j = \omega_0 + \Delta$ gives $\sqrt{J(\omega_i)J(\omega_j)} = J_0[1+(\Delta/\gamma_{\rm D})^2]^{-1/2}$, which is suppressed by a factor approximately equal to $\gamma_{\rm D}/|\Delta|$ when $|\Delta| \gg \gamma_{\rm D}$.

[48] Alexandrou A, Bianchi G, Péronne E, Hallé B, Boeuf F, André R, Romestain R and Dang L S 2001 Stimulated scattering and its dynamics in semiconductor microcavities at 80 k under nonresonant excitation conditions *Phys. Rev. B* **64** 233318

[49] Virgili T, Coles D, Adawi A M, Clark C, Michetti P, Rajendran S K, Brida D, Polli D, Cerullo G and Lidzey D G 2011 Ultrafast polariton relaxation dynamics in an organic semiconductor microcavity *Phys. Rev. B* **83** 245309